FRAGILITY ANALYSIS OF BUILDING ENVELOPE COMPONENTS SUBJECT TO WINDBORNE DEBRIS IMPACT HAZARD

A Thesis

Submitted to the Graduate Faculty of the
Louisiana State University and
Agricultural and Mechanical College
in partial fulfillment of the
requirements for the degree of
Master of Science in Civil Engineering

in

The Department of Civil and Environmental Engineering

by
Alexander H. Herbin
B.S.C.E., Louisiana State University, 2008
December 2011

ACKNOWLEDGEMENTS

First and foremost, I would like to express my unwavering gratitude towards my parents, Ruth and Robert Herbin, for the love and encouragement they have given me throughout my life. Without them, I would not be in the position I am in today. I would like to thank my major advisor Dr. Michele Barbato not only for providing me with the opportunity to pursue my graduate studies at LSU, but also for the invaluable guidance and support he has given me during my time here. Additionally, I would like to say thank you to the rest of my family and friends who were always there for me when I needed someone to talk to.

I would also like to say thank you to the other members of my advisory committee, Dr. Ayman Okeil and Dr. Steve Cai, for providing advice and assistance as needed throughout my course of study and for serving on my examining committee. Also, thank you to Dr. Marc Levitan for his support early on in my graduate studies. Thank you to Dr. Suresh Moorthy for providing his assistance and comments regarding the finite element models considered in this research and to Mr. Brian Smoorenburg for his assistance in data extraction.

Finally, I would like to thank the Longwell Family Foundation through the Fund for Innovation in Engineering Research (FIER) Program and the LSU Council on Research through the 2009-2010 Faculty Research Grant Program for funding this research.

TABLE OF CONTENTS

LIST OF TABLES

LIST OF FIGURES

ABSTRACT

This thesis presents a methodology for developing windborne debris (WBD) impact fragility curves for building envelope components (BECs) by using stochastic finite element (FE) models. These fragility curves provide the probabilistic description of the impact resistance of BECs subject to an impact event described by an appropriate intensity measure (*IM*). Accurate fragility curves are essential in the development of a general probabilistic performance-based engineering framework for mitigation of WBD impact hazard.

Monte Carlo simulation is used in combination with the FE method to propagate uncertainties in the BEC's model parameters and WBD impact location. As an application example, the fragility curves relative to different damage measures are derived for aluminum storm shutters subjected to WBD impact. It is found that (1) the missile kinetic energy at impact is a sufficient *IM* for BECs with ductile behavior subjected to WBD impact, and (2) the performance of storm panels in terms of penetration of WBDs is critically dependent on the details of the panels' installation.

1 INTRODUCTION

1.1 Motivation

The threat of natural disasters is a significant concern to society. Hurricanes, for example, frequently cause severe damage to structural and infrastructural systems in the United States of America [1],[2] and worldwide [3],[4]. This severe damage can cause enormous economic and life losses. For example, the economic loss resulting from Hurricane Katrina in 2005 was estimated to be greater than 100 billion dollars. Hurricane Katrina was also estimated to have caused more than 1500 deaths upon its landfall [5].

Approximately 50 percent of the population of the United States of America is concentrated in coastal regions and approximately 3 trillion dollars worth of infrastructure exists in these same regions [1]. To limit the damage to infrastructures, buildings, and production activities located in hurricane-prone regions, as well as the resulting economic and life losses, it is of high importance for engineers to better understand the possible impacts of hurricanes. The National Science Board (NSB) [1] identified the need for furthering the understanding of how hurricanes and structures interact and for increasing structures' resistances to hurricane loading as high priority research topics for the advancement of the nation.

1.2 Research Areas of Interest

Large tropical storms are often the cause of structural damage and loss of life. Therefore, it is important for engineers to design structures that can adequately accommodate the extreme loading produced by hurricane events (e.g., due to excess wind pressure, flooding, and/or windborne debris (WBD) impact) with an optimal use of available resources. Over the past few decades, significant advances have been achieved in risk assessment and mitigation for structures subjected to hurricane hazard [6],[7]. The advancement of structural reliability analysis and the

development of probabilistic performance-based engineering techniques have been integral to these advances. Structural reliability techniques allow the rigorous consideration of uncertainties inherent in engineering problems and are used for the calibration of design codes [8]-[10]. Probabilistic performance-based methods are extensively developed in the field of earthquake engineering [11],[12]. Similar methodologies, based on a performance-based engineering (PBE) approach, are currently being developed in other civil engineering subfields, including wind, fire, and blast engineering [13]-[17].

PBE targets the achievement of specified levels of performance for a structural system rather than following a prescriptive approach over an entire spectrum of design problems (based on general equations and calibrated coefficients, the use of which is considered sufficient to satisfy some implicitly assumed levels of performance). The aim of PBE is to ensure a sufficiently small probability, over the design life of the structure, that the damage to a structure will exceed any limit states describing failure (e.g., physical failure, member buckling), serviceability (e.g., maximum deformation, occupant comfort), and/or other performance measures [18]. In PBE, the response of a structure is described by engineering demand parameters (*EDP*s) (e.g., maximum deformation, maximum displacement, maximum force applied on a member) and is evaluated with respect to different levels of an intensity measure (*IM*). In earthquake engineering, several scalar (e.g., peak ground acceleration [18], first-mode spectral acceleration [19]) and vector *IM*s [20]-[22] have been identified and employed. In hurricane engineering, physical quantities related to mean wind speed are good candidates for use as efficient and sufficient *IM*s [14].

Performance is determined by comparing the response of the structure to appropriate damage measures (*DM*s), which are used to describe physical states of damage [12]. The PBE methodology can also provide an estimate of structural risk by determining the probability of

exceeding a given value of a decision variable (*DV)* which corresponds to a specified level of performance [23]. A *DV* is defined as a measurable quantity that represents the cost and/or benefit (e.g., monetary losses, loss of lives, downtime, and/or other factors) for the owner, the users, and/or the society resulting from the structure under consideration [12]. *DV*s for several design options can be compared in a PBE assessment analysis to guide the rational selection of a final design [23].

A critical feature of probabilistic PBE methods is the explicit consideration of uncertainties. Uncertainties can be classified into two different categories, i.e., aleatory uncertainties (due to natural variability of physical, geometrical, and mechanical properties) and epistemic uncertainties (due to lack of knowledge, imprecise modeling, and limited statistical information) [24]. Inherent randomness is virtually irreducible since it is an inevitability of nature. In contrast, epistemic uncertainties can be reduced, e.g., by implementing more accurate and realistic models. There is a great need to develop a probabilistic PBE methodology in the field of hurricane engineering since the effects of a hurricane on the built and natural environment are characterized by significant uncertainties and cannot be predicted using only deterministic models.

Among the tools developed in probabilistic PBE, a significant research interest has been focused on the construction of fragility curves [24]-[26]. Fragility curves are the cumulative distribution functions (CDFs) of the structural capacity with respect to a specific limit state, usually corresponding to a physical damage state for the structural system under consideration [27]. In hurricane engineering, only limited research has been devoted to fragility analysis [7],[28]. Thus, there is a need to develop fragility curves for structural and non-structural components of buildings. It has been shown that the building envelope is the building component

most susceptible to damage during a hurricane [7]. The building envelope consists of non-structural components such as non-load-bearing walls, windows, doors, and roofing. When the building envelope is compromised, the structure is subjected to a much higher risk of damage due to increased internal wind pressure and water penetration from rain and flooding [7],[29]. In hurricane prone regions, protection for the most critical elements in the building envelope is often installed in the form of shutters, plywood, and other types of movable reinforcement.

1.3 Objectives and Scope

The objectives of this research are (1) to propose a methodology for developing the fragility curves corresponding to representative damage states for building envelope components (BECs) and BEC protection systems subjected to WBD impact loading, and (2) to apply this methodology to BECs in order to identify appropriate *IM*s, *EDP*s, and *DM*s. The proposed methodology is based on the combination of finite element (FE) analysis and Monte Carlo simulation (MCS) [30], and is integrated into a general probabilistic PBE framework. The scope of the general methodology proposed in this research is broad in that it can be applied to any structural and/or nonstructural component. The application presented in this research, however, focuses only on ductile non-structural BECs. In the application example, fragility curves corresponding to different damage states are derived for a storm panel representative of BECs with ductile behavior, and appropriate *IM*s, *EDP*s, and *DM*s are identified as a part of this study.

1.4 Thesis Outline

Chapter 2 of this thesis presents a literature review on the background of probabilistic PBE methods, and on existing research pertaining to WBD impact on BECs such as windows and window protection systems.

Chapter 3 introduces a PBE framework for WBD impact hazard assessment and proposes a methodology, based on a combination of MCS and the FE method, for the development of fragility curves for BECs and BEC protection systems. This chapter considers the case of an aluminum hurricane protection panel subject to WBD impact as a specific application example of the proposed methodology. Within this chapter, FE modeling techniques and the modeling of parameter uncertainties are described.

Chapter 4 presents a comparison of different possible *IM*s and a discussion of results obtained from the application example in terms of *EDP*s obtained from FE analyses and relevant *DM*s identified for the BEC protection system. This chapter also includes the development of fragility curves for the aluminum hurricane protection panel with respect to the relevant *DM*s.

Finally, Chapter 5 presents conclusions and recommendations for future research.

2 LITERATURE REVIEW

2.1 Previous Research regarding WBD Impact

In the recent past, substantial research was performed regarding the performance of BECs subject to WBD impact loading. Sources of WBD were identified and classified by their flight characteristics. Additionally, important observations were reported from studies in which laboratory testing and/or numerical simulation were conducted for BECs commonly subjected to WBD impact. These studies provide valuable information regarding the performance of both unprotected annealed glass windows and aluminum hurricane protection panels under impact loading. This chapter provides a brief summary of the research results available in the literature and relevant to the study reported in this thesis.

2.1.1 Sources of WBD

In a residential area, WBD is generated from a number of different sources. These sources include, but are not limited to: roof cladding (e.g., shingles, tiles), roof and wall framing elements (e.g., 2”x4” lumber), vegetation (e.g., tree branches), road signs and signals, and any variety of items commonly found in private yards (e.g., garbage cans, mailboxes) [6],[31],[32]. Holmes [6] estimated that, in Australia, approximately 50% of WBD causing damage is generated from roof cladding elements, 10% is generated from roof framing elements, and another 10% is generated from other roof attachments. WBD damaging residential buildings often originates from roofing materials on neighboring buildings and creates a “chain reaction” of damage (as seen in post-hurricane survey of Cyclone Tracy in Australia [6]). Holmes [6] also observed that WBD that originates at higher elevations relative to the ground (i.e., at roof level) has a higher damage potential than WBD generated at lower elevations (i.e., at ground level), since it generally has a longer flight trajectory and reaches higher velocities.

WBD trajectories are of particular importance in understanding how WBD impacts occur on structures. Willis et al. [33] defined three distinct types of WBD shapes based on their flight characteristics (see Figure 1).

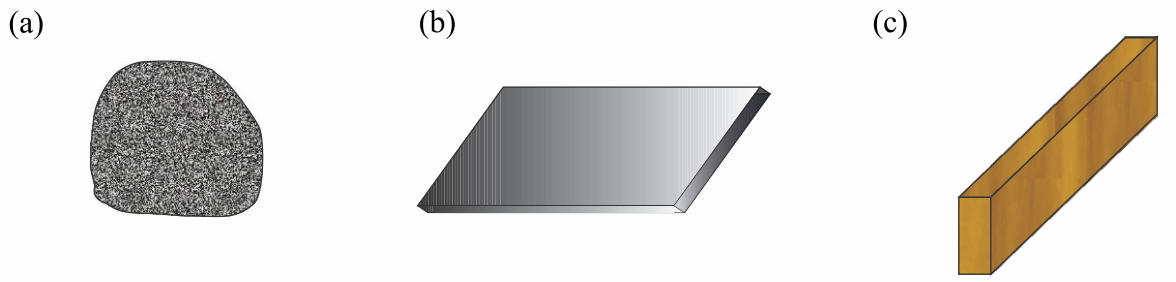

Figure 1. Types of WBD: (a) compact, (b) sheet, and (c) rod.

These WBD types are: (1) "compact" type debris, which corresponds to small, pebble like debris with no capability of achieving aerodynamic lift (see Figure 1(a)); (2) "sheet" type debris, which are wide and flat (e.g., roof shingles, roof sheathing), and can develop lift forces (see Figure 1(b)); and (3) "rod" type debris, which are long and slender (i.e., 2"x4" lumber, tree brances) and may develop lift forces, but smaller than those developed by sheet type debris (see Figure 1(c)). Figure 2 provides a graphical representation of the trajectories for these three different types of WBD. It is noted here that the research presented in this thesis is focused on the effects of 2"x4" lumber rod type WBD impact.

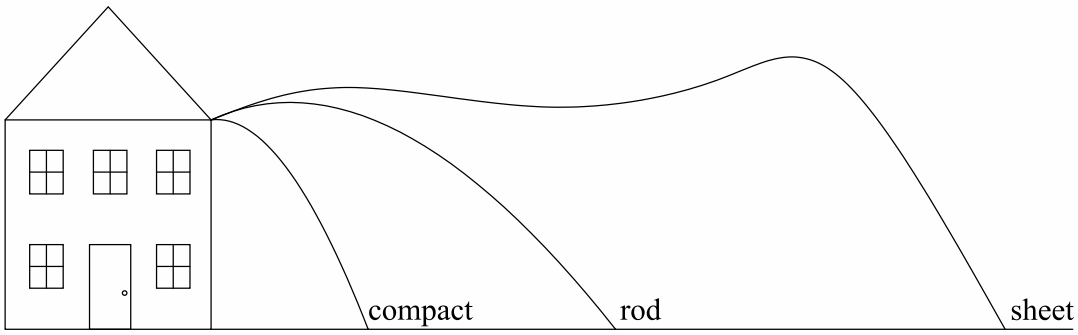

Figure 2. Typical trajectories for different types of WBD.

Willis et al. [33] determined the mathematical relationships describing the liftoff wind speeds (i.e., the wind speeds necessary for each type of WBD to achieve liftoff) by considering the balance of the forces (i.e., gravitational and aerodynamic forces) applied to potential WBD during hurricanes. For rod type WBD, the threshold wind field velocity which leads to liftoff and flight, U_{rod}, is given by:

$$U_{\text{rod}} = \sqrt{\frac{\pi}{2} \cdot (\rho_{\text{m}} / \rho_{\text{a}}) \cdot (I / C_{\text{F}}) \cdot d \cdot g} \tag{1}$$

where ρ_{m} = density of the missile material, ρ_{a} = density of the air, I = "fixture strength integrity" (i.e., a measure of the wind force required to dislodge items from a structure which can become WBD), C_{F} = aerodynamic force coefficient, d = effective diameter of the missile (i.e., the diagonal dimension of a 2"x4" missile), and g = gravitational acceleration constant. Using this equation, Willis et al. [33] estimate that wind speeds in excess of 32 m/s (i.e., approximately 72 mph) will cause a typical 2"x4" lumber missile of length 2.400 meters to achieve liftoff.

Based on wind tunnel and full case tests, the flight trajectories of sheet debris are studied in [34], and the flight trajectories of compact and rod debris are studied in [35]. It was found in [34] and [35] that the maximum horizontal velocities achieved by these three types of types of WBD are described by a function of the WBD horizontal flight distance, mass, and drag properties. Lin et al. [35] found that for rod type debris (i.e., corresponding to a 2"x4" missile of length 2.400 m and weight of 4.100 kg) the ratio of horizontal missile speed to wind field velocity, u_{m}/U, could be approximated as:

$$\frac{u_{\text{m}}}{U} \approx 1 - e^{-\sqrt{0.058x}} \tag{2}$$

where x is the horizontal displacement of the missile. A plot of equation (2) over a possible flight distance of 100 m is provided in Figure 3.

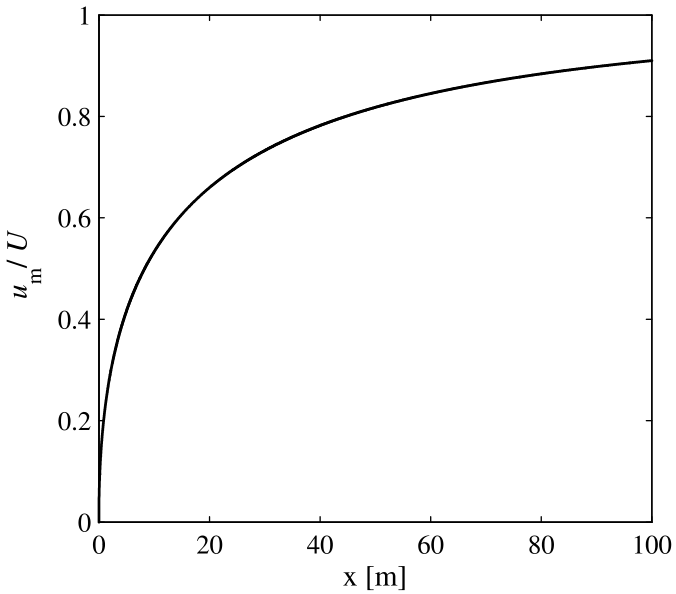

Figure 3. Ratio of horizontal missile speed to wind field velocity for rod type WBD as a function of flight distance.

From Figure 3, it is observed that largest acceleration of rod type 2"x4" lumber WBD occurs in the first 5 to 10 meters of flight in which the WBD can reach approximately 30-50% of the wind field velocity. With knowledge of the average distance between buildings (i.e., average flight distance of WBD) in a given hurricane prone area, an approximation of the range of u_m possible for a 2"x4" lumber missile in that area is attainable. Knowing the minimum velocity level that induces WBD flight (i.e., U_{rod} in equation (1)), Figure 3 can be used to give an approximation of u_m for any magnitude of $U \geq U_{rod}$.

2.1.2 WBD Impact on BECs with Brittle Behavior

Vulnerability of window glass to WBD impact has attracted the interest of several researchers. However, only a few studies focused on the development of fragility curves for brittle BECs (e.g., annealed glass windows). In a study performed by the NAHB research center [36], annealed glass window samples of different sizes and thicknesses were subjected to 4.600 pound (i.e., corresponding to a mass of 2.087 kg) 2"x4" missile (i.e., rod type WBD) impacts at

varying levels of missile impact linear momentum (LM_{m}). The missiles considered in this study were representative of WBD generated from roof framing elements in a hurricane. In order to assess the fragility of the annealed glass specimens, several window specimens were tested at multiple levels of LM_{m}. The probability of failure was recorded as the ratio of the number of windows which broke after one missile impact and the total number of trials N at each level of LM_{m}. The results obtained from [36] indicated that a 100% probability of window failure was reached at $LM_{\mathrm{m}} = 7.198\,\mathrm{kg}\cdot\mathrm{m/s}$ for 61cm x 61cm, 2.380 mm thickness window specimens, and at $LM_{\mathrm{m}} = 8.096\,\mathrm{kg}\cdot\mathrm{m/s}$ for 61cm x 61cm, 3.970 mm thickness window specimens.

Masters et al. [32] used laboratory experiments to assess the vulnerability of double-strength annealed glass to impact by different types of debris with different impact orientations. The tests considered 61cm x 61cm glass specimens with thickness of 3.180 mm, and debris types commonly found in post-storm surveys, including rod type wooden dowel missiles of diameter 2.540 cm and 5.080 cm and mass equal to 200g. These missiles were intended to simulate tree limbs and other vegetation which become WBD during a hurricane. In order to build a "vulnerablility curve" (i.e., a fragility curve, using the terminology of PBE), N = 20 window specimens were tested at multiple levels of LM_{m} (i.e., 20 window specimens per level of LM_{m}) for the case corresponding to head-on impact using the two types of dowels. Through these tests, it was found that unprotected glass specimens impacted by lightweight rod type WBD present almost a 100% failure probability for values of the impact linear momentum as low as $LM_{\mathrm{m}} = 4\,\mathrm{kg}\cdot\mathrm{m/s}$ [32]. The differences in the LM_{m} levels corresponding to 100% probability of failure for the similar brittle BEC specimens tested in [32] and [36] suggest that the types of WBD impacting brittle BECs influence their fragilities in terms of LM_{m}.

The fragility curves obtained in [32],[36] are among the first probabilistic descriptions of BEC performance under WBD impact and show that brittle BECs are extremely vulerable to damage from rod type WBD impacts even at low levels of LM_{m}. The results presented in these studies also suggest that WBD impact protection systems are essential to ensure acceptable levels of performance by structures located in hurricane prone areas

2.1.3 WBD Impact on BECs with Ductile Behavior

The research available in the literature regarding the performance of BECs with ductile behavior subjected to WBD impact is also scarce. Borges et al. [37] numerically studied the performance of aluminum and steel storm shutters subject to WBD impact based on the Miami Dade County test protocols. In this study, a deterministic FE model was used to simulate WBD impact. This FE model considered storm shutters mounted on a fixed rail system along two sides and left unconstrained along the other two sides. The following observations were made: (1) material failure is not observed in any trials due to the high level of flexibility in the model and the impact energy dissipation through panel deformation; (2) the highest level of damage is recorded in impacts occurring along the unrestrained outer boundaries of the panels and corresponding to the missile passing the panel and coming into unrestricted contact with the protected BEC with brittle behavior; and (3) the applied boundary conditions and the geometry of the panel significantly affect the response of the panel in terms of deformations [37].

Fernandez et al. [31] assessed the performance of storm shutters subject to WBD impact experimentally. In their study, the effect of impacts of different sources of WBD were considered, namely roof tiles and 9 lb 2”x4” missiles. The impact velocities for all trials were fixed at a value of 15.250 m/s. Boundary conditions corresponding to a track mounting system were considered. The following conclusions were made: (1) WBD impacts near the panels’

corners (i.e., near the track boundary conditions) can damage the panels in a “pull-out” or “push-through” pattern (i.e., the panels can break at the connection between the track and the panels themselves and can be either pushed through or pulled out of the mounting track). (2) Debris of the same weight and impact velocity but of different shapes and impact orientations can cause different levels of damage when impacting storm shutters. (3) Commonly accepted 2”x4” lumber impact testing standards may be insufficient to ensure that a storm panel satisfying the requirements of the standards also achieves a target level of performance, since impact velocities are likely to exceed 15.250 m/s and missile types are not uniform during a design level hurricane event [31]. These results suggest that current best practices are not able to account for the typical variability observed in WBD impact during hurricane events and, thus, an alternative methodolgy is needed to ensure a satisfactory performance of BECs and BEC protection systems.

2.2 Building Code Requirements for BECs Subject to WBD Impact

The 2012 edition of the International Building Code [38] requires that glazing elements on structures located in hurricane prone regions must be protected by an impact resistant covering or be impact resistant themselves. According to the IBC, the performances of these impact resistant BECs must be assessed using the ASTM E1996 and ASTM E1886 test standards [39],[40]. The IBC also mandates that glazing elements located less than 30 feet above grade (i.e., indicative of most small residential construction) must be tested using the “large missiles” (i.e., 9 lb 2”x4” missiles) defined in [39]. An impact resistant BEC must pass these tests to be allowed for use in hurricane prone regions. A range of typical WBD impact velocities during hurricanes is identified as 9 to 30 m/s (i.e., approximately 20 to 70 mph) in [40]. According to the protected

structure's location relative to the coastline, a WBD impact test velocity is prescribed by the standards.

The testing methods described in [39] and [40] consist of subjecting an impact resistant BEC to WBD impact at prescribed locations on its surface and then to cyclical pressure loading (i.e., cycling from positive to negative pressures) to simulate the real conditions the BEC will experience during a hurricane [40]. The impact locations considered in the testing correspond to the center of the BEC and a corner of the BEC near its boundary conditions. The testing methods require the BECs be installed according to the manufacturer's specification, i.e., there are no standard requirements for the details of BEC installation given in [39] and [40]. To accept an impact resistant BEC for use, these standards only require a number of performance metrics to be satisfied based on the prescribed test impact types and pressure loading. Therefore, it is seen that the existing building codes and test standards are prescriptive in nature and do not account for the uncertainty inherent to hurricane induced hazards.

2.3 Probabilistic and Reliability-Based Methods in Structural Engineering

Modern design methods, such as the Load and Resistance Factor Design (LRFD) method [37], generally have probabilistic (reliability-based) foundations. However, these methods are prescriptive in nature and are not suitable to satisfy explicitly specified levels of performance.

Probabilistic approaches for direct assessment of WBD risk are relatively recent, e.g., compared to similar approaches in earthquake engineering. One of the first models for assessment of the risk of failure of glazing components due to WBD impact was developed by Twisdale et al. [6],[41]. A simplified version of this model was implemented in the HAZUS software to predict the risk of damage to a glazing element during a given period of time, T, during a hurricane event [6]. The probability of damage, P_D, is given as:

$$P_D = 1 - \exp\{-N \cdot A \cdot T \cdot [1 - F_{\xi}(\xi_D)]\} \quad (3)$$

in which N = average number of impacts per unit time and unit surface area, A = surface area of the glazing components, $F_{\xi}(\xi_D)$ = CDF of kinetic energy or linear momentum, and ξ_D = kinetic energy or linear momentum beyond which the glazing component is damaged. While this approach represents a significant advancement toward PBE compared to ordinary prescriptive approaches proposed in design codes, it neglects important sources of uncertainty (e.g., variability of the damage threshold) and, thus, presents serious limitations when applied to design of structures subjected to WBD hazard.

Another application of probabilistic and performance-based techniques to hurricane engineering is found in Li and Ellingwood [7]. In their proposed framework, first order reliability methods were used to probabilistically describe performance of building components. Uncertainty in wind speed modeling was considered by using three different models in the analysis and comparing the final results. Each model used a Weibull distribution with different site specific distribution parameters to describe the wind speed. Conducting first order reliability analyses of controlling limit state functions at increasing levels of the *IM* yielded fragility curves for roof and cladding elements. The fragility curves for each component were developed using hurricane 3 second gust speed at 33 feet above ground in exposure category C, taken from [42], as the *IM*. These fragility curves proved to fit lognormal distributions with low sampling errors. By convolving the fragility models with wind speed models, the probability of failure of a component, P_f, was obtained as:

$$P_f = \int_0^{\infty} F_R(v) \cdot f_v(v) \cdot dv \quad (4)$$

in which $F_R(v)$ = structural fragility, and $f_v(v)$ = probability density function (PDF) of hurricane wind speed v. This approach represents a significant step forward toward the development of a PBE methodology for wind and hurricane engineering.

2.4 State of the art PBE Methods

Structures that are located in different geographical regions are inherently subjected to different levels of risk due to different sources with different expected magnitudes of natural hazards. Existing design and building codes account for the different hazard sources and their variability (e.g., ASCE 7 maps for wind, earthquake, and snow loads [42]), and employ reliability-based procedures to ensure implicit levels of performance with respect to safety and serviceability. However, a prescriptive approach to design presents several limitations [43]. Evaluating the relative effectiveness with respect to a given performance requirement of multiple proposed designs that are all acceptable based on code prescriptions is difficult if not impossible. Additionally, prescriptive code requirements present a road block to design innovation and cannot be directly applied to design of structures under conditions in which there is no previously existing knowledge [14]. Therefore, applying prescriptive building codes, design standards, and mitigation techniques to all structures regardless of type and location is not always appropriate [44].

It is recognized that the most rational approach for structural design considering risk due to natural phenomena is through the use of PBE methodologies [44]. In PBE, the aim is to achieve specified levels of performance for structural designs, rather than designing a structure to withstand prescribed loading conditions. A design is acceptable if the probability that it does not satisfy a specified limit state is sufficiently low. This criterion removes many of the restrictions of a prescriptive approach and allows engineers to identify an optimal structural design among a

set of many possible designs for a given problem [14]. PBE methods also allow for the explicit consideration of uncertainties in structural loading resulting from highly unpredictable natural phenomena (e.g., earthquakes, hurricanes) and uncertainties in structural capacity emanating from variability in mechanical and geometrical properties [24]. Under these considerations, PBE methods have been adopted in several modern seismic design codes [45],[46].

The Pacific Earthquake Engineering Research (PEER) Center's performance-based earthquake engineering (PBEE) method is a general and widely accepted example of probabilistic PBE based on the total probability theorem [11],[12],[23],[44]. The PEER method aims to evaluate performance at both the component and system level in terms of *DV*s such as structural response, repair costs, and deaths (i.e., dollars, deaths, and downtime [12]) after an earthquake using a series of independent analysis phases which consider four different quantities (i.e., *IM*, *EDP*, *DM*, *DV*) which fully describe the design problem. Additionally, the PEER PBEE methodology rigorously accounts for uncertainties affecting each phase of the analysis, e.g., component fragility and ground motion variability [12]. Performance is evaluated by estimating the probability that specific levels of *DV*s will be exceeded for a specific structure subjected to seismic hazard. This methodology can be used to build the probability distributions of the potential losses to stakeholders of the structure in question. Overall, extensive research results available in the literature have shown that the use of PBEE methods can lead to more accurate loss estimation and more efficient design for structures subject to seismic excitation [23],[47]-[50].

2.4.1 Identification of *IM*s

In PBE, *IM*s serve as a link between hazards and structural response. In order to obtain an accurate probabilistic estimate of the response of a structure subject to, for example, seismic

loading, an appropriate (i.e., sufficient and efficient) *IM* must be identified for the structure in question. Significant research has been conducted to determine sufficient and efficient *IM*s for use in PBE methodologies [19]-[22]. In the context of PBEE, an *IM* is said to be sufficient when it renders an *EDP* independent of the earthquake's magnitude and site to source distance. An *IM* is said to be efficient when its use produces a small variance in the *EDP* [19]. In studies about sufficiency and efficiency of *IM*s, it was found that no single *IM* is sufficient and efficient for all types of structures. Different *IM*s have been identified for different types of structures by using several different methods, including time history analysis of nonlinear FE models of structures subjected to selected historical ground motions. In these studies, it is concluded that the determination of a structure specific appropriate *IM* is an integral part of a PBE methodology [19]-[22].

2.4.2 Fragility Analysis

Fragility analysis is the component of a probabilistic PBE approach in which fragility curves (or fragility functions) are derived. Fragility functions provide the probabilistic representation of the structural capacity of a structure or of a structural component with respect to a specific limit state and correspond to the CDFs of *DM*s conditional to specific values of the corresponding *EDP*s [12]. An important element of fragility analysis is the identification of the pertinent limit states for a given structure or structural component.

Fragility functions are often found or assumed to follow lognormal distributions [51]. In this case, the level of *EDP* corresponding to a given probability of structural damage, *p*, can be determined from a fragility function represented by a lognormal CDF as follows [51]:

$$X_p = x_m \cdot \exp(\beta \cdot \Phi^{-1}(p)) \tag{5}$$

where X_p = value of *EDP* describing a probability of damage p, x_m = mean of the distribution, β = log standard deviation of the distribution, and $\Phi^{-1}(p)$ = inverse of the standard normal CDF for probability p.

In the field of earthquake engineering, a significant research effort has been conducted regarding fragility analysis, including a number of past studies focused on deriving fragility functions for structures and structural components [24]-[27],[51]-[53]. Porter et al. [52] noted that fragility functions can be obtained from either empirical or theoretical data. In [52], fragility functions for structural and nonstructural components of a welded steel moment frame building subject to seismic excitation were derived using both empirically and theoretically obtained data available in the literature describing building components of interest. In Beck et al. [53], fragility functions were derived for reinforced concrete beam-columns subject to seismic excitation corresponding to a number of damage states ranging from light damage to collapse. These fragility functions were derived from existing empirical data regarding the failure of these types of structural components. From these fragility functions, fragility curves (see Figure 4) were plotted with respect to the displacement damage index, *DDI* (i.e., *EDP* = *DDI*), defined as the structural damage resulting only from member displacements (i.e., curvatures) during earthquake loading. Taken from the Park-Ang damage index, the *DDI* is calculated as follows:

$$DDI = \frac{\Phi_m - \Phi_r}{\Phi_u - \Phi_r} \tag{6}$$

where Φ_m = maximum curvature achieved by the beam-column under loading, Φ_r = recoverable curvature after unloading of the beam-column, and Φ_u = nominal ultimate curvature capacity of the beam-column.

From Figure 4, it is observed that, as the magnitude of the *EDP* increases, the possible damage states become more severe and the damage probability increases.

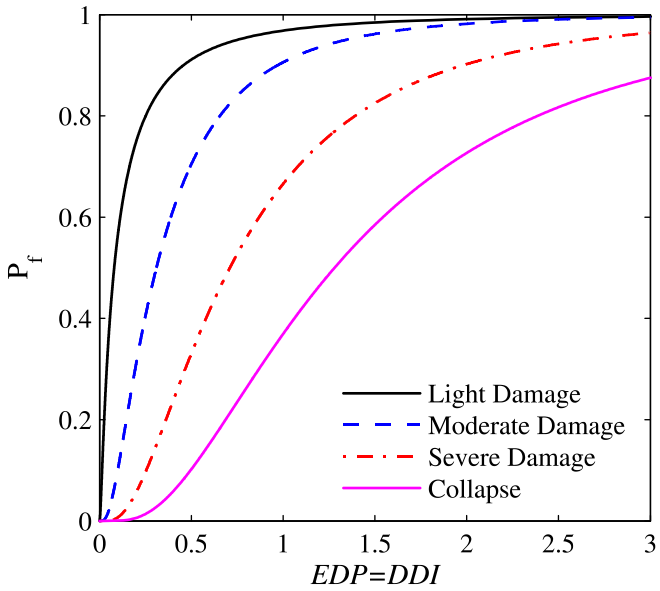

Figure 4. Example fragility curves relative to multiple damage states for concrete beam-columns subject to seismic excitation (adapted from [53]).

2.4.3 Extension of PBE to Hurricane Engineering

An extension of the PEER PBEE methodology was proposed for hurricane engineering by Barbato et al. [23]. This extension is referred to as performance-based hurricane engineering (PBHE) and accounts for the different sources of hazard (i.e., wind pressure, flooding, WBD impact, and rainfall) related to hurricane landfalls in hurricane prone areas. In addition, the PBHE framework accounts for the uncertainties related to the "environment" (i.e., the region not affected by the presence of the structure), the "structure", and the "exchange zone" (i.e., the region in which natural actions interact with the structure).

3 METHODOLOGY

This chapter presents the PBE framework for assessment of WBD impact risk and illustrates the methodology adopted to build the fragility curves for BECs with ductile behavior. In addition, a detailed description of the deterministic FE model and of the uncertainties affecting the performance of the BEC is provided.

3.1 Introduction

This research proposes to adapt the probabilistic PBE framework developed by PEER for earthquake engineering to hurricane engineering problems, with particular emphasis on the assessment and mitigation of WBD impact risk. This framework has as theoretical basis in the total probability theorem. A crucial component of this research is the identification of appropriate *IM*s that are sufficient and efficient [54] as well as *EDP*s and *DM*s describing the structural response parameters and damage states, respectively, that are relevant to assess the risk due to WBD impact. The focus of this research is the development of fragility curves for BECs subjected to WBD impact.

These fragility curves are constructed using results obtained from stochastic FE models that account for inherent uncertainties in both the BECs and in the location of WBD impact. The stochastic FE approach adopted in this research consists of building a set of FE models with the parameters' values obtained from MCS. From the mechanical response of the FE models of the BECs subjected to WBD impact, the statistics of the relevant *EDP*s are computed and used to fit a theoretical CDF to the simulation results. In the damage analysis phase, relevant damage states are identified and the statistical description of the corresponding *DM*s is obtained, based on available data and/or on engineering judgment. Finally, the statistical description of the *EDP*s and *DM*s are convolved to derive the fragility curves for the *DM*s of interest.

The methodology described here is very general and can be applied to any structural component, non-structural component, and/or system subjected to WBD impact hazard. It is clear that every different component/system will require the definition of different *IM*s and will be described by different *EDP*s and *DM*s. Compiling an exhaustive list of possible *IM*s, *EDP*s, and *DM*s is beyond the scope of this research. In this research, the proposed methodology is illustrated for the specific problem of an aluminum storm panel (which is representative of BECs with ductile behavior) subjected to WBD impact hazard.

3.1.1 Total Probability Theorem

The total probability theorem allows the computation of the probability of occurrence of an event, *A*, by using conditional probabilities [55]. Considering a set of *n* mutually exclusive and collectively exhaustive events E_i $(i = 1, 2, \ldots, n)$ (i.e., events that cannot occur simultaneously, and having a sum of their probabilities equal to one), and given the conditional probabilities $P(A|E_i)$ $(i = 1, 2, \ldots, n)$, the total probability theorem can be stated as follows:

$$P(A) = \sum_{i=1}^{n} P(AE_i) = \sum_{i=1}^{n} P(A|E_i) \cdot P(E_i) \tag{7}$$

where $P(AE_i)$ = probability of simultaneous occurrence of events *A* and E_i.

In the context of probabilistic PBE, uncertainties are characterized in terms of continuous random variables. Given two continuous random variables *X* and *Y*, the total probability theorem gives the complementary cumulative distribution unction (CCDF) of *X*, $G_X(x)$ as:

$$G_X(x) = \int_{-\infty}^{\infty} G_{X|Y}(x|y) \cdot f_X(y) \cdot dy \tag{8}$$

where $G_{X|Y}(x|y)$ is the CCDF corresponding to the probability of *X* being greater than or equal to *x* subject to the condition $Y = y$ [15].

3.1.2 Adopted PBE Methodology

The methodology adopted in this paper is derived from the PBEE framework developed by PEER. The PEER PBEE method is a general and widely accepted example of probabilistic PBE based on the total probability theorem [11],[12],[23]. The PEER PBEE framework computes the mean annual frequency of exceeding a specific level of a *DV* at a specific location, $g[DV]$, as:

$$g[DV] = \iiint p[DV \mid DM] \cdot p[DM \mid EDP] \cdot p[EDP \mid IM] \cdot g[IM \mid D] \cdot \mathrm{d}IM \cdot \mathrm{d}EDP \cdot \mathrm{d}DM \quad (9)$$

in which $p[A|B]$ = probability density function (PDF) of random variable *A* conditional on a specified value of random variable *B*, and $g[A]$ = mean annual frequency of variable *A* outcrossing a specified value. The analysis is decomposed into four phases that must be conducted sequentially. A flowchart describing the PEER PBEE methodology is provided in Figure 5. The parameters used in any step are chosen so that they remain independent of those from all previous steps [23].

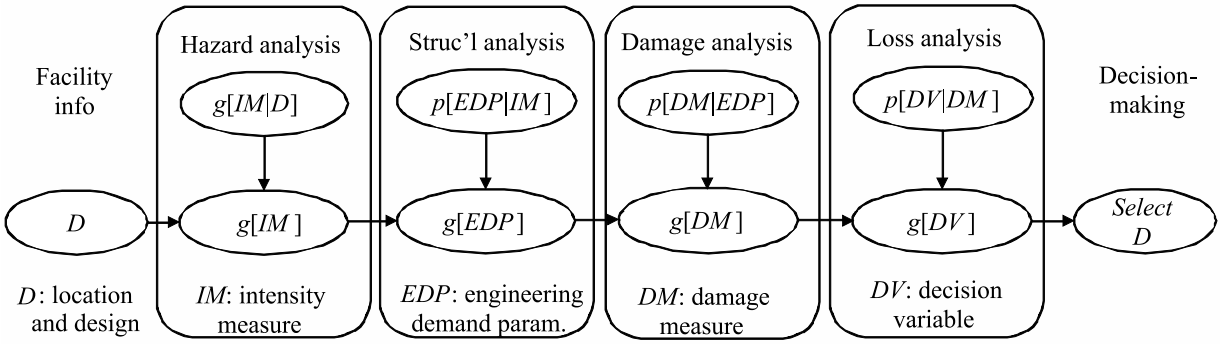

Figure 5. PEER methodology flowchart.

The first phase is known as hazard analysis and consists of defining a hazard curve or hazard function, $g[IM]$, for the specific location of the structure. The hazard function defines the frequency in which different levels of intensity of the hazard considered are exceeded in a given time frame. In the second phase, referred to as structural analysis, a structural model is used to determine the PDF of the *EDP*(s) conditional to knowledge of *IM*, i.e., $p[EDP|IM]$. The third

phase, referred to as damage analysis, is used to determine the fragility functions that describe the probability of exceeding a specific limit state represented in the form of a *DM* conditional to knowledge of *EDP*, i.e., $p[DM|EDP]$. Decision variables (*DV*) related to structural damage are then considered in the loss analysis phase, yielding $p[DV|DM]$ in Eq. (9).

3.2 Description of Physical Specimen

BEC protection options readily available for practical applications include different types of hurricane shutters, e.g., Bahama shutters, colonial shutters, and storm panels. This research considers corrugated aluminum hurricane panels, which are chosen over other options based on their relatively low cost and ease of installation. The geometrical schematics for this type of hurricane protection are readily available. The aluminum panels are made of 0.05" (1.27 mm) gauge 3004 H34 type aluminum.

A picture of the storm panel's physical specimen is shown in Figure 6(a). The test missiles are 2"x4" (nominal dimensions: 5.080 cm and 10.160 cm) pieces of pine wood lumber (with actual dimensions after curing and finishing of 1.5 in (3.810 cm) and 3.5 in (8.890 cm)) weighing 9, 12, and 15 pounds (corresponding to masses of 4.082, 5.443, and 6.804 kg), which represent the typical missiles recommended for use in the ASTM E1996 Standard [39]. This standard specifies the minimum required performance for protective systems which are impacted during extreme wind events. According to the standard, such elements must be able to withstand the impact of a 9 pound 2"x4" missile traveling at 90 ft/s (27.432 m/s). Thus, it is clear that the ASTM E1996 Standard requirements correspond to a prescriptive approach, which does not explicitly consider the uncertainties of WBD impact.

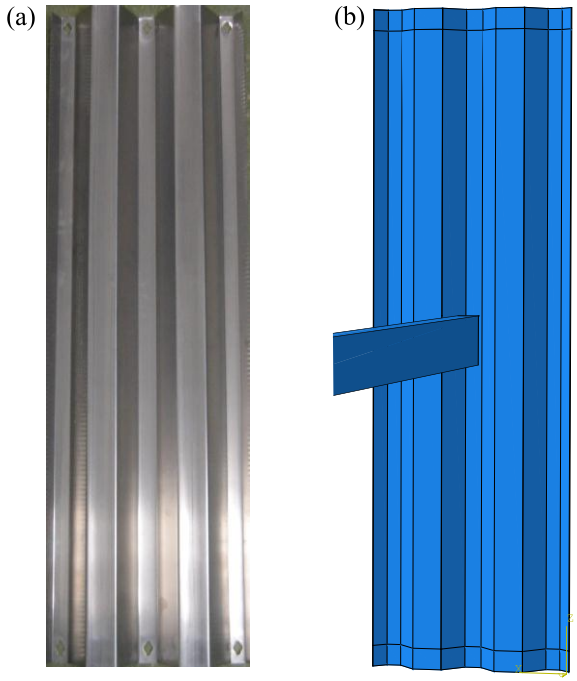

Figure 6. Aluminum storm panel: (a) picture of a physical specimen, and (b) ABAQUS FE model.

3.3 Finite Element Modeling

The commercially available FE program ABAQUS [56] is employed in this research to perform the nonlinear FE dynamic impact analyses required to estimate the effects of WBD impact on the storm panel. ABAQUS is chosen for its flexibility and extensive modeling options. Within ABAQUS, a complete model can be constructed using built-in CAD capabilities. ABAQUS also provides the user with several solution algorithms and a vast database of element types. Critical features of ABAQUS pertaining to WBD impact modeling include its capabilities for dynamic impact analysis and for nonlinear FE analysis, including both nonlinear material behavior and nonlinear geometry [56].

The three-dimensional geometrical representation of the two different model parts (i.e., the aluminum panel and the wood missile) is obtained by extrusion of the technical drawings of the panel's cross-section (obtained from the producer's website [57], see Figure 7(a)) and the cross-

section of a 2”x4” lumber missile. Each part is modeled using material constitutive models readily available in the ABAQUS library. The wood constituting the missiles is modeled as a linear elastic material, while the storm panel’s aluminum is modeled using an isotropic hardening material model (similar to the material model used in Roeder and Sun [58], in which impact of steel projectiles on aluminum/alumina laminates was studied). This modeling choice is based on the fact that isotropic hardening is generally more significant for problems involving high levels of plastic strain for a single load cycle (like the ones considered in this research) when compared to kinematic hardening effects, which can become more important in modeling the mechanical response of materials subjected to cyclic loadings with large hysteresis cycles. The parameters used to define the material constitutive models of wood and aluminum are shown in Table 1.

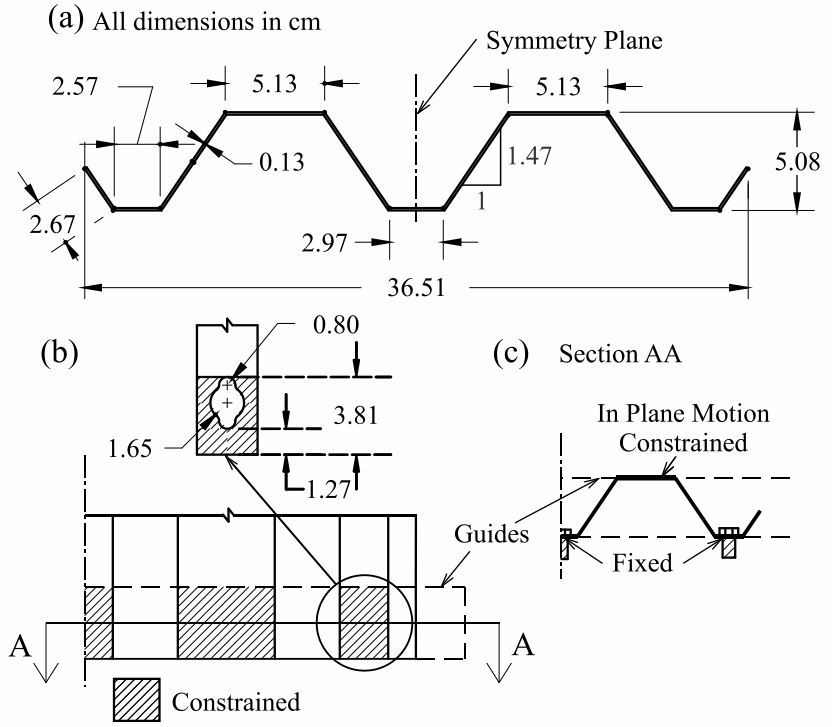

Figure 7. Aluminum storm panel: (a) panel cross section, (b) boundary conditions corresponding to the considered installation, and (c) details of the installation and corresponding physical constraints.

Once the model’s individual parts are defined, they are assembled into a three-dimensional FE model using the ABAQUS CAE assembly module (see Figure 6 (b)). One of the panel’s

corners is located at the origin of the global coordinate system to ensure that the panel's local coordinates correspond to the model's global coordinates. This allows for easy relocation of the missile's impact point from trial to trial. The boundary conditions of the panel component are imposed in order to simulate the mounting of the panel on a fixed rail system, which represents a common installation option (see Figure 7(b)). The top and bottom edges (i.e., the shorter sides) of the panel are fixed (i.e., the nodal displacements are constrained to be equal to zero in all three coordinates) and the portions of the panel that are in direct contact with the mounting system are constrained to allow motion only in the plane of the panel. These boundary conditions correspond to the connection between the panel and the rail system which is provided through the use of bolts (see Figure 7(c)). The left and right sides (i.e., the longer sides) of the panel are modeled as unconstrained. A predefined initial velocity field (before impact) is applied to the missile. Surface contact between the different components (i.e., the panel and the missile) is modeled using the penalty contact algorithm [56],[59]. The contact surfaces in the model are taken to be the entire surface of the missile as one surface and the entire surface of the aluminum panel as the other surface.

The standard brick three-dimensional (3D) hexahedral C3D8R (3D continuum element with 8 nodes and reduced integration) element with enhanced hourglass control and linear displacement interpolation in each direction is chosen for building the 3D FE model of the panel and the missile. This element type is readily available in the ABAQUS library and is preferred to wedge and tetrahedral elements due to its higher accuracy for the same mesh size and faster convergence rate when the FE mesh is regular (i.e., the shape deformation of the element is small) [56]. A selectively-reduced integration scheme is used to control volumetric locking, which can develop in fully integrated hexahedral elements for incompressible materials and can

cause displacements to be underestimated. This scheme fully integrates deviatoric strain terms and underintegrates volumetric strain terms using a single integration point [60]. Using this type of integration scheme, however, can lead to hourglass modes developing during an analysis. Hourglassing occurs in elements with only one integration point if the deformation of an element results in the calculation of zero strain at the integration point during the analysis. In ABAQUS, hexahedral reduced integration elements have built in hourglass mode stabilization control, and in the case of models which include nonlinear materials, it is recommended to enable enhanced hourglass control to provide greater resistance to hourglass modes [56]. The model mass is defined by assigning to each material a mass per unit volume, the values of which are given in Table 1.

Table 1: Statistical characterization of model parameters.

Parameter	Units	Mean	COV	Distribution	Min	Max
Missile: Pine Wood						
Density	kg/m^3	494.252	-	-	-	-
Young's Modulus	GPa	8.963	-	-	-	-
Poisson's Ratio	-	0.387	-	-	-	-
Panel: 3004H34 Aluminum						
Density	kg/m^3	2720.935	-	-	-	-
Young's Modulus	GPa	68.948	10	Normal	-	-
Poisson's Ratio	-	0.350	-	-	-	-
Yield Strength	MPa	199.948	10	Normal	-	-
Ultimate Strength	MPa	241.317	10	Normal	-	-
Strain at Rupture	-	0.120	-	-	-	-
Missile Impact Location						
X Impact Location	cm	-	-	Uniform	0	36.513
Y Impact Location	cm	-	-	Uniform	0	120.015

ABAQUS uses the defined density to calculate the inertia properties of the FE model using a lumped mass formulation, i.e., the total mass obtained from the volume of the FEs and the corresponding material density is concentrated in the individual nodes of each element during the dynamic FE analysis [56].

3.4 Dynamic Finite Element Impact Analysis

WBD impact is analyzed with ABAQUS by using the nonlinear dynamic FE analysis technique. The FE model is analyzed using the explicit central-difference direct integration scheme [56]. WBD impact is simulated using an automatic time incrementation scheme, which ensures global stability of the time integration scheme. The duration of the time history is chosen so that both the peak response at impact and the vibration response after impact can be examined. Results are reported at 0.0005 s intervals, allowing for the accurate representation of the dynamic response of the panel. Both material and geometric nonlinearities are included in the analysis.

A FE mesh sensitivity study is performed to ensure that the FE results obtained in this research are independent of the mesh size. A first FE mesh sensitivity study is performed by considering geometric nonlinearities only, i.e., by modeling the aluminum material of the panel as a linear elastic material. This study is used to estimate the range of mesh sizes of interest for the fully nonlinear model. Figure 8 shows the nodal displacement time histories recorded at the center of the panel, Δ_{ctr}, and corresponding to mesh sizes of 0.500", 0.330" and 0.250" (1.270, 0.838, and 0.635 cm respectively) for the FE model with nonlinear geometry and linear materials. Here, the mesh size is defined as the maximum dimension of any single hexahedral brick element in any direction. It is observed that the Δ_{ctr} time histories are very close for all the meshes considered. In particular, the response of the FE model with nonlinear geometry and linear materials is no longer sensitive to the mesh at sizes of 0.250" or smaller.

The mesh sensitivity study is then repeated for the fully nonlinear FE model. Figure 9 shows nodal displacement time histories recorded at the center of the panel, Δ_{ctr}, and corresponding to mesh sizes of 0.500", 0.330", 0.250", and 0.125"(1.270, 0.838, 0.635, and 0.318 cm respectively) for the FE model with nonlinear geometry and linear materials. It is observed that

the Δ_{ctr} time histories obtained from the model with mesh size equal to 0.250" and the model with mesh size equal to 0.125" have a difference of less than 3% in the peak values of Δ_{ctr}, and of less than 4% in the residual plastic deflection.

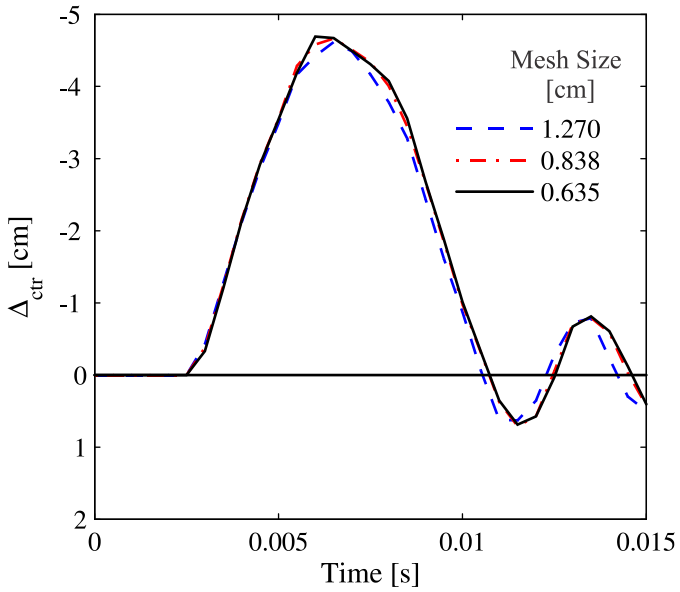

Figure 8. Mesh convergence study for FE model with nonlinear geometry and linear materials.

A mesh size of 0.250" is chosen for the remainder of the FE analyses performed in this study, since the computational cost of a single analysis increases exponentially with decreasing mesh size (i.e., 1 hour and twenty minutes CPU time for 0.250" mesh over a 0.0250s time history versus 8 hours CPU time for 0.125" mesh over the same time history using a 64 bit Dell Precision T3400 machine with 4 GB of RAM, running on two of four cores available in a 2.40 GHz Intel Core 2 Quad Q6600 quad core CPU). This computational cost increase is prohibitive for probabilistic PBE applications, while the response time histories obtained with a mesh size of 0.25" are deemed accurate enough for engineering application. The FE model which is used in the remainder of this research has a total of 19,411 elements, 38,104 nodes, and 114,312 degrees of freedom (DOFs). The FE response is simulated over a 0.030s time history to ensure the accurate representation of the panel's plastic deflection.

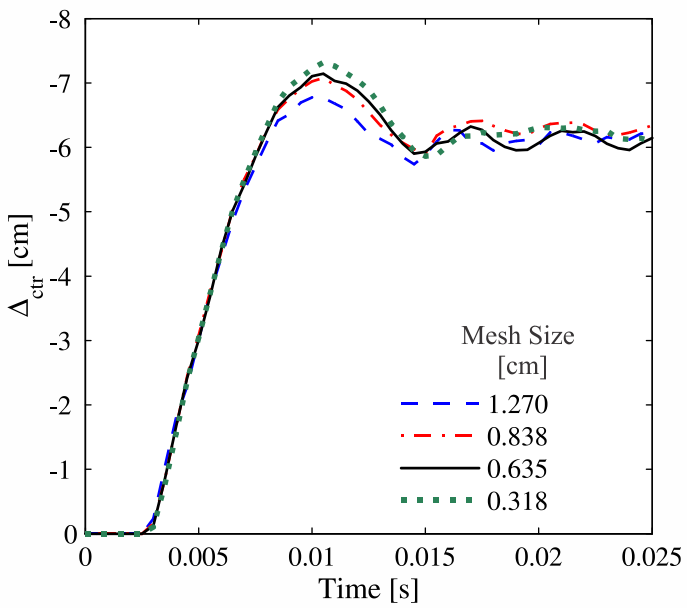

Figure 9. Mesh convergence study for fully nonlinear FE model.

3.5 Modeling of Parameter Uncertainty

The FE models employed to estimate the *EDP*s' statistics are built using the sampled values of the model parameters obtained through MCS. This research considers the uncertainties in both the material properties of the aluminum panels and the location of the WBD impact. The modulus of elasticity, yield stress, and ultimate strength of aluminum are modeled as normally distributed random variables, while the aluminum Poisson's ratio and strain at rupture, as well as the pine wood mechanical properties and the material densities of both aluminum and wood are modeled as deterministic quantities. The effects of space variability of these uncertain quantities are not considered in this research. The X and Y coordinates of the missile impact location (defined as the location of impact of the geometric center of the 2"x4" section of the missile) are represented as uniform random variables. The values of the model parameters modeled as deterministic quantities as well as the statistical description of the parameters modeled as random variables are provided in Table 1. Mean values of the aluminum random mechanical properties are obtained from [61], while the pine wood elastic modulus and mass density are taken from

[62]. Due to the lack of statistical information regarding the mechanical properties of 3004 H34 aluminum, the types of probability distributions and the coefficients of variation (COVs) are selected based on engineering judgment and information regarding similar metallic materials. All random parameters are modeled as statistically independent random variables.

4 RESULTS AND DISCUSSION

4.1 Determination of an Appropriate *IM*

PBE applications require the identification of a sufficient and efficient *IM*. Three possible choices of *IM*s are considered here: (1) the missile impact velocity, V_m, (2) the missile impact linear momentum, LM_m, and (3) the missile impact kinetic energy, KE_m. These potential *IM*s are evaluated for sufficiency by using a deterministic FE model for WBD impact analysis with material parameters set at their mean value and a constant point of impact corresponding to the center of the panel. This model is referred to as the "mean model". Impacts are simulated at various levels of the possible *IM*s, by considering missiles of three different weights, i.e., 9, 12, and 15 pounds (corresponding to masses of 4.082, 5.443, and 6.804 kg), and by varying the velocity of the WBD impacts.

From each dynamic FE analysis, the values of the following two *EDP*s are recorded: (1) the maximum total deflection of the storm panel during impact, Δ_{max}, and (2) the maximum plastic deflection of the storm panel after impact, Δ_{pl}. The *EDP* values are extracted from the FE model's output database through ABAQUS CAE. Δ_{max} is computed as the maximum displacement in the direction of impact over the entire response time history for all nodes of the panel's FE model. This *EDP* is chosen because it is related to the possible damage to the windows protected by the storm panel. Δ_{pl} is defined as the largest residual displacement after impact in the direction orthogonal to the plane of the panel. This *EDP* is chosen because it is related to the possible damage to the storm panel itself. The values of Δ_{max} and Δ_{pl} recorded for the mean model are denoted as Δ_{max}^0 and Δ_{pl}^0, respectively. A typical time history of the deflection of a node of the mean model during the dynamic impact analysis is shown in Figure 10. This node is chosen as node # 15,310, with coordinates X_{15310} = 15.390 cm and Y_{15310} = 60.330 cm

(i.e., close to the center of the panel). Figure 10 also shows the values of the total deflection ($\Delta^0_{max,15310}$) and of the plastic deflection ($\Delta^0_{pl,15310}$) for node # 15,310.

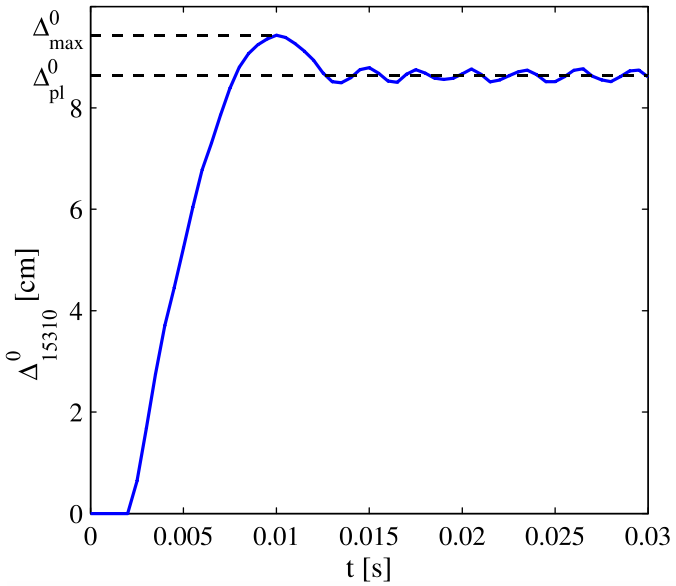

Figure 10. Typical time history of the nodal deflection along the impact direction (node #15,310).

The *EDP* values for the mean model are plotted versus their corresponding *IM* values in Figure 11 through Figure 13 in order to determine the sufficiency of the three potential *IM*s considered in this research. In particular, Figure 11 plots the *EDP*s as functions of V_m, Figure 12 plots the *EDP*s as functions of LM_m, and Figure 13 plots the *EDP*s as functions of KE_m. It is observed that both Δ^0_{max} and Δ^0_{pl} present a significant scatter when V_m and LM_m are used as *IM*. In fact, the *EDP*s are dependent on V_m and LM_m (with an approximately linear functional dependency) and on the weight of the missile. In contrast, the values of the two *EDP*s are practically independent of the weight of the missile when KE_m is used as *IM*. Thus, KE_m is identified as the only sufficient *IM* (among the three potential *IM*s considered here) for the *EDP*s considered in this research.

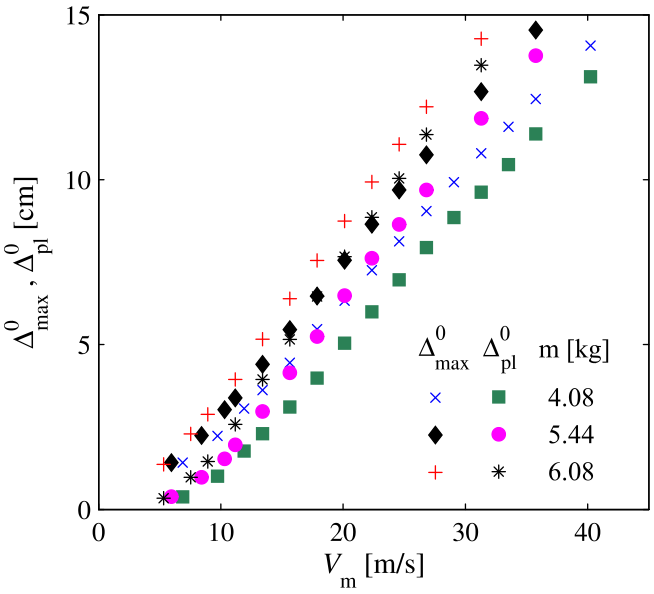

Figure 11. *EDP*s' values for the mean model considering V_m as *IM*.

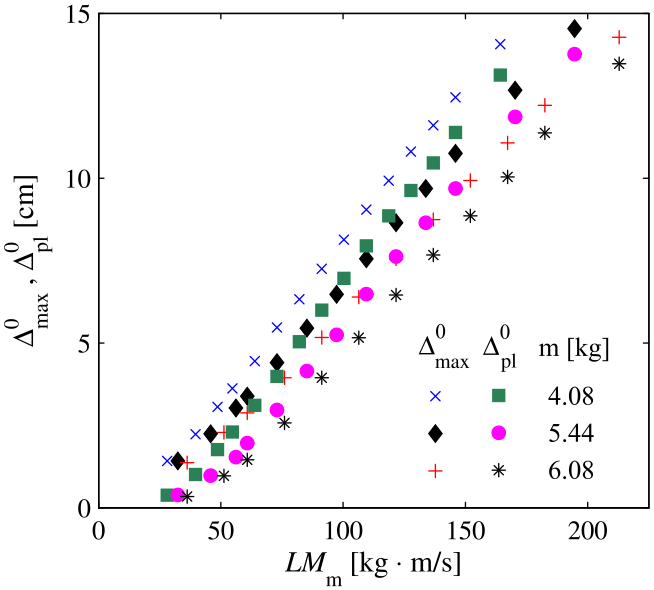

Figure 12. *EDP*s' values for the mean model considering LM_m as *IM*.

It is found that, for values of KE_m larger than 0.250 kJ, Δ^0_{max} and Δ^0_{pl} can be expressed as quadratic functions of KE_m. The following relations are found by using a least-square fitting procedure for $KE_m \geq 0.250$ kJ and by adding a quadratic interpolation curve for $0\,\text{kJ} \leq KE_m < 0.250\,\text{kJ}$:

$$\Delta_{\max}^{0} = \begin{cases} -25.345 \cdot \left(KE_{\mathrm{m}}\right)^{2} + 18.460 \cdot KE_{\mathrm{m}} & 0 \le KE_{\mathrm{m}} < 0.250 \\ -0.713 \cdot \left(KE_{\mathrm{m}}\right)^{2} + 6.144 \cdot KE_{\mathrm{m}} + 1.540 & KE_{\mathrm{m}} \ge 0.250 \end{cases} \quad \left[\text{units: cm, kJ}\right] \quad (10)$$

$$\Delta_{\mathrm{pl}}^{0} = \begin{cases} -1.675 \cdot \left(KE_{\mathrm{m}}\right)^{2} + 6.903 \cdot KE_{\mathrm{m}} & 0 \le KE_{\mathrm{m}} < 0.250 \\ -0.745 \cdot \left(KE_{\mathrm{m}}\right)^{2} + 6.438 \cdot KE_{\mathrm{m}} + 0.058 & KE_{\mathrm{m}} \ge 0.250 \end{cases} \quad \left[\text{units: cm, kJ}\right] \quad (11)$$

The fitting curves given in Eqs. (10) and (11) are shown in Figure 13. The quadratic fitting provides a very good representation of the results obtained from the FE analyses. This finding suggests that the *EDP-IM* relations $\Delta_{\max}^{0}$ - KE_{m} and Δ_{pl}^{0} - KE_{m} can be estimated with sufficient accuracy using only three FE analyses.

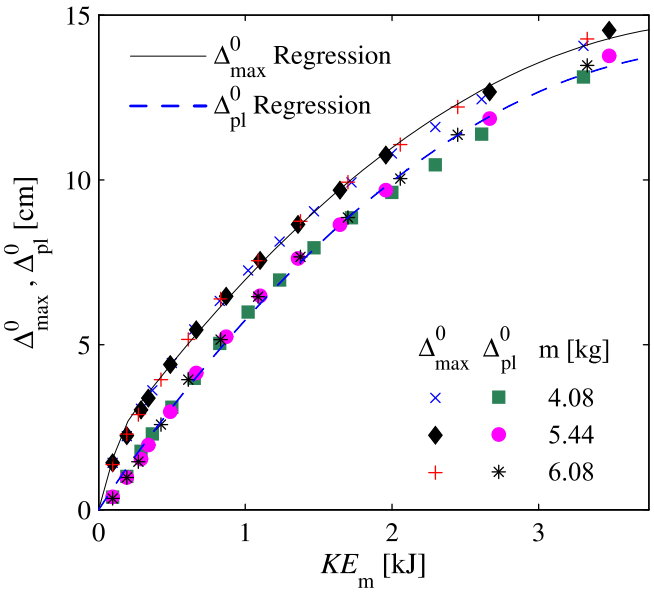

Figure 13: *EDP*s' values for the mean model considering KE_{m} as *IM*.

Based on the results obtained, it is inferred that KE_{m} is an appropriate *IM* for BECs with ductile behavior. This result is consistent with results recently made available in the literature [6]. It is noted here that most of the studies currently available in the literature are focused on WBD impact on glass and/or other BECs with brittle behavior and suggest the use of LM_{m} as *IM* for these types of BECs [32],[36] .

4.2 Structural Analysis Results and Statistical Characterization of the *EDP*s

In the structural analysis phase, the statistical description of the *EDP*s conditional to the value of the identified *IM* (i.e., KE_m) is obtained by using stochastic FE analysis for the BECs subjected to WBD impact. A statistically representative number of samples of the random parameters are obtained using MCS for each level of *IM*. The sampled values of the parameters are used as input to define the different sample FE models. Based on preliminary FE analyses, a number of 100 simulations per *IM* level is selected in order to identify an appropriate distribution for the fragility curves with an adequate accuracy for engineering applications. The different levels of the *IM* are obtained by using only one missile weight (i.e., 15-pound missile) and by varying the velocity of the missile. The results of 100 simulations for each random variable considered in the model corresponding to impact intensity of KE_m = 0.612 kJ and with the boundary conditions shown in Figure 7 are shown in APPENDIX A.

4.2.1 Identification of Impact Typologies

Figure 14 and Figure 15 plot the experimental CDFs for Δ_{max} and Δ_{pl}, respectively, for different levels of KE_m (i.e., KE_m = 0.272, 0.612, 1.088, 1.700, 2.447, and 3.331 kJ). Each CDF is obtained from the results of 100 stochastic FE analyses at a specific level of *IM*. Three distinct regions can be identified in each of these experimental CDFs. The first region corresponds to a concentration of FE analyses resulting in very small values of Δ_{max} and Δ_{pl}. The second region includes FE analyses which provide values of Δ_{max} and Δ_{pl} that are more spread out. Finally, the third region in the experimental CDFs corresponds to the FE analyses in which the missile penetrates the storm panel. In this thesis, these impacts are referred to as "penetrations". For these FE analyses, it is not possible to identify specific values of Δ_{max} and Δ_{pl} and only the number of penetrations observed at each level of *IM* can be recorded. These numbers of

penetrations are reported in Figure 14 and Figure 15. It is observed that the numbers of penetrations do not significantly vary for different levels of KE_m.

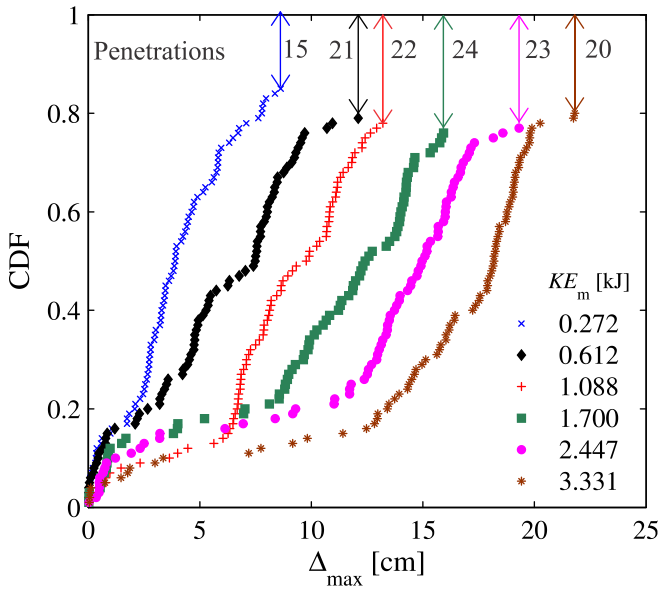

Figure 14. Experimental CDFs for Δ_{max} including all types of impacts.

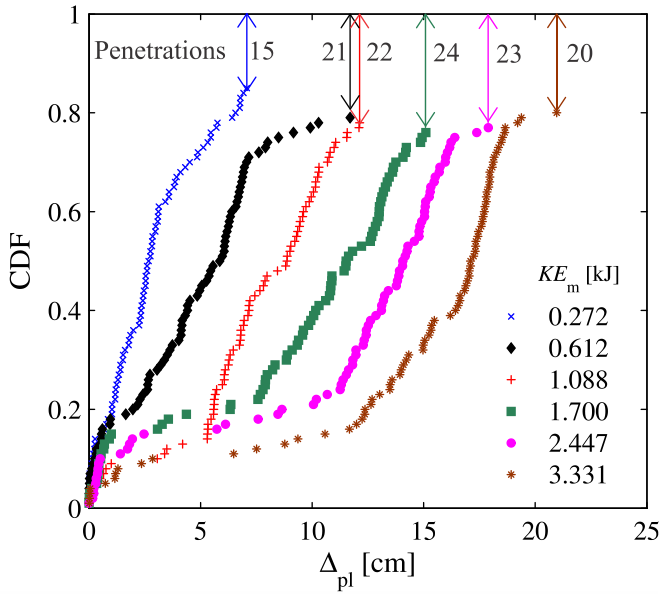

Figure 15. Experimental CDFs for Δ_{pl} including all types of impacts.

The experimental CDFs shown in Figure 14 and Figure 15 can be better interpreted by analyzing the WBD impact locations and the corresponding impacts' characteristics. In

particular, it is observed that the recorded values of Δ_{max} and Δ_{pl} are usually very small when the impact locations belong to the portion of the storm panel where the fixed boundary conditions are applied (including an additional rectangular area along the short side of the panel of width equal to one half of the height of the 2"x4" missile, i.e., 4.445 cm). These impacts are referred to as "boundary impacts" in this thesis, since the values of the *EDP*s critically depend on the boundary conditions applied. The main effect of these boundary impacts is a net reduction in the vulnerable area of the panel, assuming that the wall on which the panel is attached is not vulnerable to damage from WBD impact. More generally, the values of the *EDP*s for boundary impacts depend not only on the storm panel's properties, but also on the properties of the structural component on which the storm panel is installed. In contrast, when the impacts do not occur on this portion of the storm panel and are not penetrations, larger values of Δ_{max} and Δ_{pl} are usually recorded. In this thesis, these impacts are referred to as "ordinary impacts". Figure 16 shows the impact locations on the storm panel and the corresponding impact types (i.e., boundary impacts, ordinary impacts, and penetrations) of 100 FE analyses with random material properties and random impact locations for 15-pound missiles impacting at 30, 50, and 70 mph (i.e., for KE_m = 0.612, 1.700, and 3.331 kJ, respectively). It is noteworthy that the impact locations of the penetrations are concentrated in the portions of the storm panel which are located near the unconstrained sides. The dimensions of these portions are practically constant for all the values of KE_m, and can be approximately identified with two symmetric parabolic segments with basis b = 103.510 cm and height h = 6.350 cm (see Figure 16). The sum of the areas of these two parabolic segments correspond to 20.0% of the area of the panel, which is very close to the average ratio between the number of penetrations and the total number of impact analyses estimated over all values of KE_m considered in this research (i.e., 20.8%, with 125 penetrations

out of 600 FE simulations). 101 of the 125 penetrations recorded are located within these two symmetric parabolic segments. These observations suggest that penetration is dependent on impact location and boundary conditions rather than intensity of the WBD impact and variability of the storm panel's material properties.

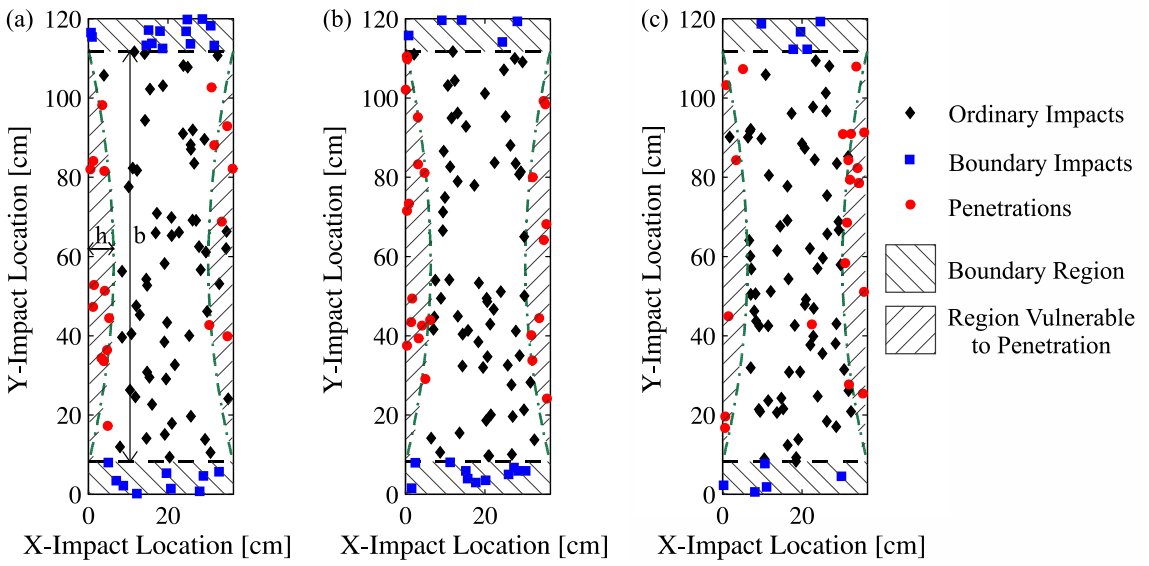

Figure 16. Impact locations and corresponding impact types: (a) KE_m = 0.612 kJ, (b) KE_m = 1.700 kJ, and (c) KE_m = 3.331 kJ.

4.2.2 Statistical Characterization of the *EDP*s for Ordinary Impacts

The variability of the *EDP*s corresponding to ordinary impacts is also of interest. New experimental CDFs are obtained considering only the values of the *EDP*s obtained from the ordinary impacts (i.e., by eliminating the results corresponding to the boundary impacts and the penetrations, and then by normalizing the probability of the remaining results to 1). From these values, the means and standard deviations for Δ_{max} and Δ_{pl} are computed at the different levels of KE_m. The normal, lognormal, and truncated normal (with lower truncations at Δ_{max} = 0 cm and Δ_{pl} = 0 cm, respectively) distributions are compared in order to find the best fit to the ordinary impacts' results. This comparison is performed by using the modified Kolmogorov-Smirnov goodness-of-fit test [63], which accounts for the fact that the distributions' parameters are

estimated from the data. Figure 17 illustrates the experimental CDF for *EDP* Δ_{max}, and the theoretical CDFs corresponding to KE_m equal to 0.612 kJ (i.e., to 15-pound missiles impacting at 30 mph) for all considered distributions. Figures presenting the experimental and theoretical CDFs for Δ_{max} and Δ_{pl} for all considered levels of KE_m are presented in APPENDIX B.

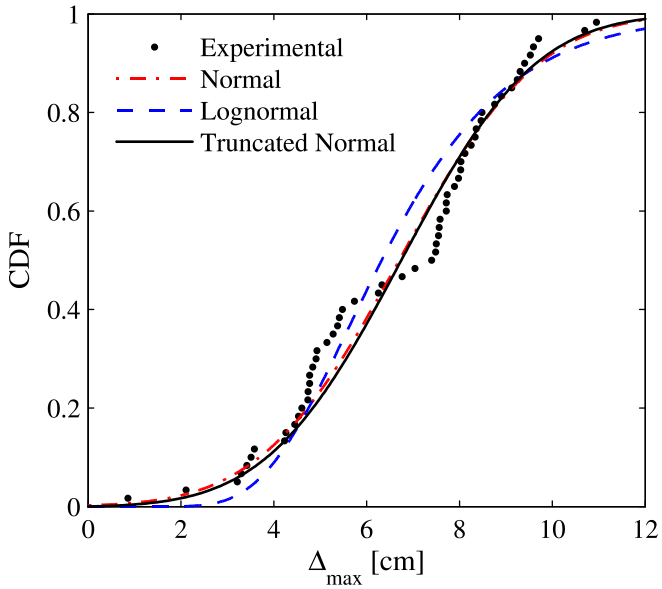

Figure 17. Experimental and fitted CDFs of Δ_{max} for ordinary impacts and KE_m = 0.612 kJ.

In the modified Kolmogorov-Smirnov test, the proposed distribution is accepted at a given significance level, α, if the maximum difference between the experimental CDF and the theoretical CDF, D_n, is less than the critical value, $D_{n,\alpha}$, corresponding to the given level of significance [55]. If multiple distributions are acceptable at a given significance level, a more detailed statistical analysis (e.g., involving the use of the method of matching moments, maximum likelihood tests, and/or probability plots [55],[63]) is needed to decide the best fit. Table 2 presents the results of the modified Kolmogorov-Smirnov testing on the reduced data sets at a significance levels α = 5% and α = 1%. The critical $D_{n,\alpha}$ values are obtained from [63]. In Table 2, bolded D_n values indicate that the considered probability distribution is acceptable at

α = 5% significance, and underlined D_n values indicate that considered probability distribution is acceptable at α = 1% significance.

Table 2: Modified Kolmogorov-Smirnov test results for the probabilistic characterization of the *EDP*s corresponding to ordinary impacts.

KE_m [kJ]	N	Observed D_n (Δ_{max} - Δ_{pl})			Critical D_n	
		Distribution			α	
		Normal	Lognormal	Truncated Normal	.05	.01
0.272	66	0.117-0.160	**0.063-0.100**	**0.078**-0.112	0.109	0.127
0.612	60	0.117-**0.086**	0.178-0.129	**0.114-0.085**	0.114	0.133
1.088	69	0.111-**0.096**	0.132-0.125	0.113-**0.099**	0.107	0.124
1.700	60	**0.113-0.102**	0.135-0.133	0.118-**0.111**	0.114	0.133
2.448	62	**0.074-0.085**	**0.093**-0.122	**0.069-0.084**	0.113	0.131
3.331	70	0.158-0.163	0.188-0.196	0.164-0.160	0.106	0.123

It is observed that (1) at 5% significance, many of the data sets can be represented by normal or truncated normal distributions, while in only three cases a lognormal distribution can be accepted; and (2) at 1% significance, a normal or truncated normal distribution is acceptable in most of the cases (with the exception of the largest value of KE_m for both normal and truncated normal distribution, and of the smallest value of KE_m and Δ_{pl} for the normal distribution), while a lognormal distribution is acceptable only in two cases out of six for Δ_{max} and in four cases out of six for Δ_{pl}. Thus, the lognormal distribution is excluded as a possible fit for the data, and the truncated normal distribution is preferred over the normal distribution because it avoids physically impossible negative values of Δ_{max} and Δ_{pl}.

Figure 18 compares the mean values of Δ_{max}, $\mu(\Delta_{max})$, corresponding to the ordinary impacts in the probabilistic FE model simulations and the Δ_{max}^0 curve given in Eq. (2). Figure 18 also shows the values of $\mu(\Delta_{max})$ plus/minus one standard deviation, $\sigma(\Delta_{max})$, as well as the minimum and maximum values of Δ_{max} recorded over all the FE analyses performed (denoted as "Min" and "Max", respectively, in Figure 18).

It is observed in Figure 18 that the curve $\mu(\Delta_{max})$ is consistently higher than Δ^0_{max}, and the minimum and maximum values of Δ_{max} show a significant dissymmetry when compared with the $\mu(\Delta_{max})$ curve (i.e., the difference between the $\mu(\Delta_{max})$ and the Min curve is significantly larger than the difference between the $\mu(\Delta_{max})$ and the Max curve). The standard deviation $\sigma(\Delta_{max})$ increases at a slower rate than $\mu(\Delta_{max})$ as KE_m increases, i.e., the COV (i.e., the ratio $\sigma(\Delta_{max})/\mu(\Delta_{max})$) significantly decreases (from 0.414 to 0.186) in the $0.272\,\text{kJ} \le KE_m < 3.331\,\text{kJ}$ range.

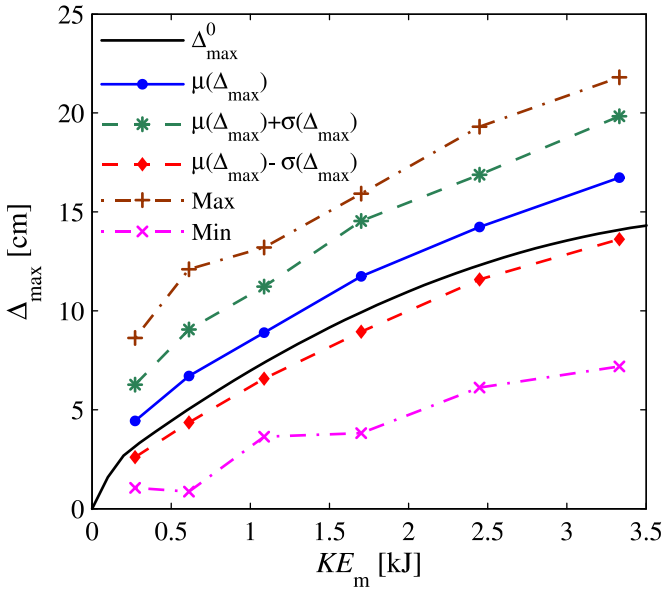

Figure 18. Comparison of Δ^0_{max} and statistics of Δ_{max}.

It is observed that the two curves $\mu(\Delta_{max}) - \sigma(\Delta_{max})$ and Δ^0_{max} are close in the same KE_m range. The difference between the mean *EDP* $\mu(\Delta_{max})$ and the *EDP* of the mean model, Δ^0, can be represented as normalized discrepancy $\delta(\Delta)$, defined as:

$$\delta(\Delta) = \frac{\mu(\Delta) - \Delta^0}{\sigma(\Delta)} \tag{12}$$

in which Δ denotes Δ_{max} or Δ_{pl}, and Δ^0 denotes Δ^0_{max} or Δ^0_{pl}. It is observed that $\delta(\Delta_{max})$ assumes values close to about 70% over the considered KE_m range. The last observation suggests that it may be possible to obtain an approximate estimate of the mean and standard deviation from the Δ^0_{max} curve.

Figure 19 compares the Δ^0_{pl}, $\mu(\Delta_{pl})$, $\mu(\Delta_{pl}) + \sigma(\Delta_{pl})$, and $\mu(\Delta_{pl}) - \sigma(\Delta_{pl})$ curves and shows the minimum and maximum values of Δ_{pl} recorded over all the FE analyses performed. Similar observations can be made for Δ_{pl} as those made for Δ_{max} in Figure 18. In particular, the coefficient of variation $\sigma(\Delta_{pl})/\mu(\Delta_{pl})$ decreases from 0.551 for $KE_m = 0.272\,\text{kJ}$ to 0.185 for $KE_m = 3.331\,\text{kJ}$, and the normalized discrepancy $\delta(\Delta_{pl})$ remains close to about 80% over the considered KE_m range. Table 3 reports the values of the mean, standard deviation, COV, and normalized discrepancy for both Δ_{max} and Δ_{pl}.

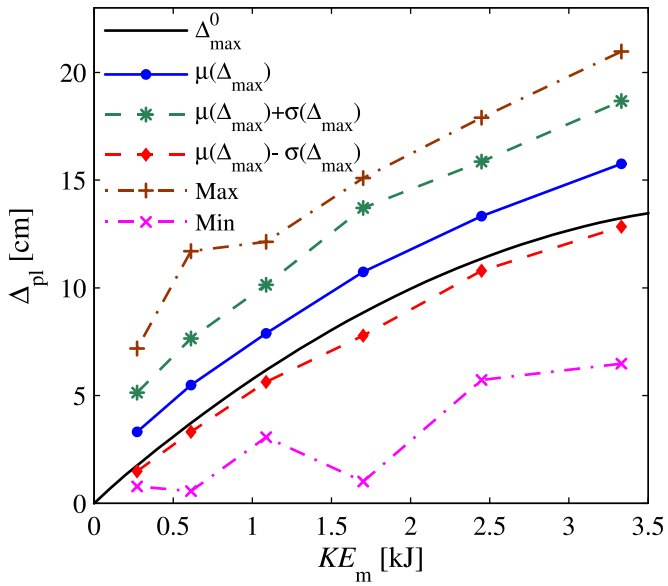

Figure 19. Comparison of Δ^0_{pl} and statistics of Δ_{pl}.

Table 3: Statistics of *EDP*s.

KE_m [kJ]	μ [cm]		σ [cm]		COV [%]		δ [%]	
	Δ_{max}	Δ_{pl}	Δ_{max}	Δ_{pl}	Δ_{max}	Δ_{pl}	Δ_{max}	Δ_{pl}
0.272	4.44	3.31	1.84	1.82	41.4	55.1	69.6	85.3
0.612	6.70	5.48	2.35	2.17	35.0	39.6	71.1	81.2
1.088	8.90	7.89	2.33	2.25	26.2	28.6	65.2	75.8
1.700	11.74	10.74	2.80	2.96	23.8	27.6	64.9	64.1
2.448	14.23	13.33	2.65	2.53	18.6	19.0	72.7	78.1
3.331	16.73	15.76	3.10	2.92	18.6	18.5	84.8	86.5

4.3 Effects of Impact Location Variability and Boundary Conditions

The effects of the impact location variability and boundary conditions are studied by performing 100 FE analyses for KE_m = 1.088 kJ (i.e., for a 15-pound missile impacting the panel at 40 mph): (1) with random impact locations (with the same probability distributions as described in Table 1) and the same boundary conditions described in Figure 2, but with deterministic material parameters (with values set equal to their means, see Table 1); and (2) with random impact locations and material parameters (with the same probability distributions as described in Table 1), but different boundary conditions (see Figure 20). The new boundary conditions correspond to the same installation previously considered (i.e., the mounting of the panel on a fixed rail system); however in this case, the storm panel that is wider than the opening required for the window and it overlaps the installation wall by 0.5 in (1.270 cm) along the two unconstrained sides of the panel. The portions of the wall that overlap with the installed panel are explicitly incorporated into the FE model in order to simulate the effects of the contact between the deformed panel subject to WBD impact and the wall. The wall is considered sufficiently strong to tolerate impact without damage (a hypothesis that represents a reasonable approximation for brick and/or concrete walls) and is modeled as a rigid component by constraining all DOFs of the corresponding FE portion. In order to simulate the impact between the deformed panel and the rigid wall, two new surface-to-surface contact pairs are defined between the panel and the new portion of the FE model representing the wall.

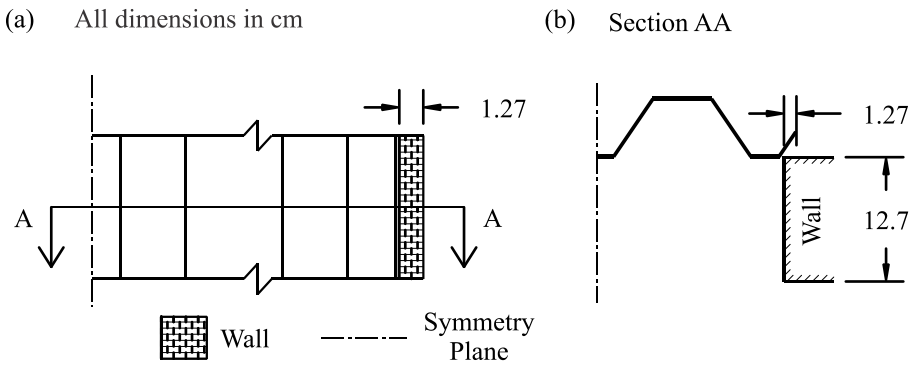

Figure 20. Boundary conditions corresponding to storm panel wider than window opening (New BCs case): (a) front view, and (b) section view.

Figure 21 shows the impact points and the corresponding impact type with KE_m = 1.088 kJ for the case (1) with random material properties and impact locations and original boundary conditions (referred to as "Original Model") in Figure 21(a); (2) with random impact locations, deterministic material parameters and original boundary conditions (referred to as "Deterministic Material") in Figure 21(b); and with random impact locations and material parameters but new boundary conditions (referred to as "New BCs") in Figure 21(c).

For the Deterministic Material case, 27 penetrations are recorded out of the 100 FE simulations, compared to the 22 penetrations recorded for the portion in the Original Model case. 22 of the 27 penetrations (i.e., 81.5%) occur within the two symmetric parabolic segments previously identified as the storm panel's portions that are vulnerable to penetration. For the New BCs case, only four penetrations are recorded out of the 100 FE simulations. This reduction of the number of penetrations is very significant, since it is obtained with a relatively small modification of the boundary conditions which can be easily implemented in practical applications (e.g., by introducing into building codes minimum requirements on the overlap between walls and storm panels). The storm panel's portion where the missile impacts can be classified as boundary impacts (i.e., impacts producing very small deflections due to the boundary conditions in the FE model) is significantly larger when compared to the Original

Model case. In fact, in addition to the two regions at the top and at the bottom of the panel identified in the Original Model case, this portion includes two additional regions located along the unconstrained sides of the panel which have a width equal to the width of the overlap between the wall and the storm panel plus one half of the width of the missile (i.e., 3.175 cm). From Figure 21(c), it is observed that three of the four recorded penetrations in the New BCs case occur within the region defined as the difference between the two symmetric parabolic segments identified as vulnerable to penetration in the Original Model case and the new region with boundary impacts. The impact location of the fourth penetration is also very close to the vulnerable region identified above. The previous observations confirm that penetration of storm panels is strongly dependent on the missile's impact location and storm panel's boundary conditions, while it is only weakly dependent on the variability of the storm panel's material properties.

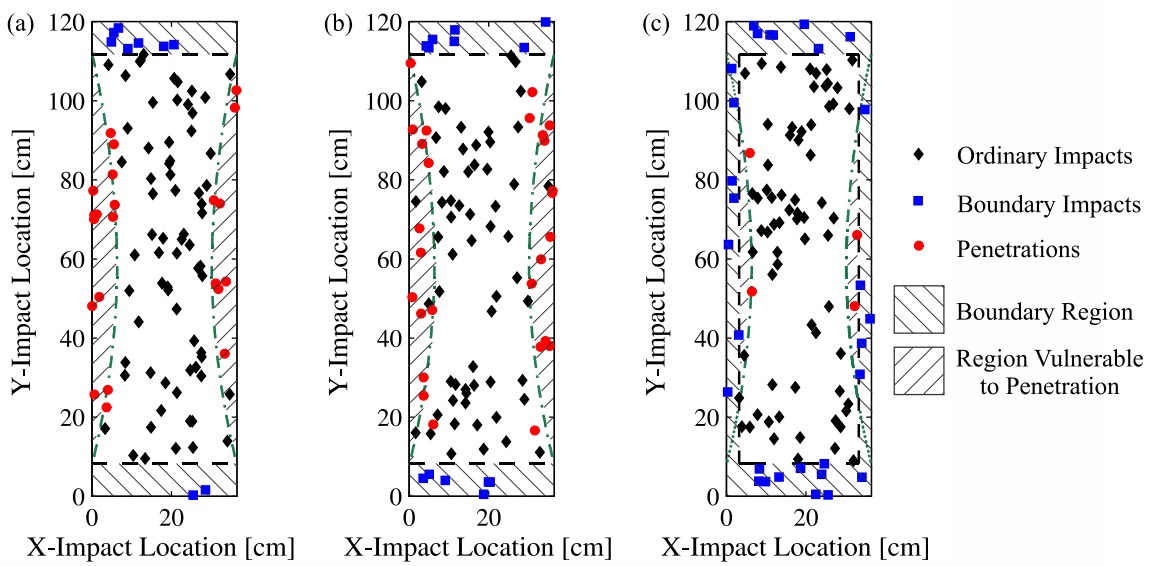

Figure 21. Impact locations and corresponding impact types for KE_m = 1.088 kJ: (a) Original Model case, (b) Deterministic Material case, and (c) New BCs case.

Figure 22 and Figure 23 compare the experimental CDFs of the *EDP*s Δ_{max} and Δ_{pl}, respectively, relative to KE_m = 1.088 kJ and corresponding to ordinary impacts for the Original Model, Deterministic Material, and New BCs cases.

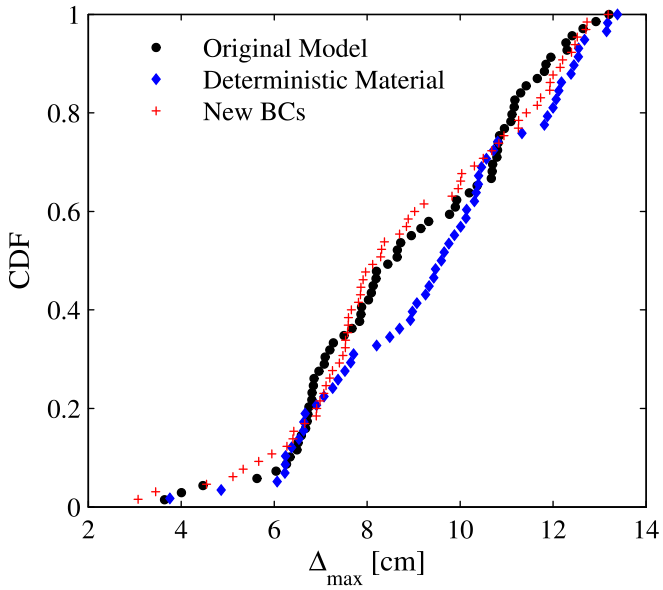

Figure 22. Effects of boundary conditions and material variability on the experimental CDFs of Δ_{max} for ordinary impacts and KE_m = 1.088 kJ.

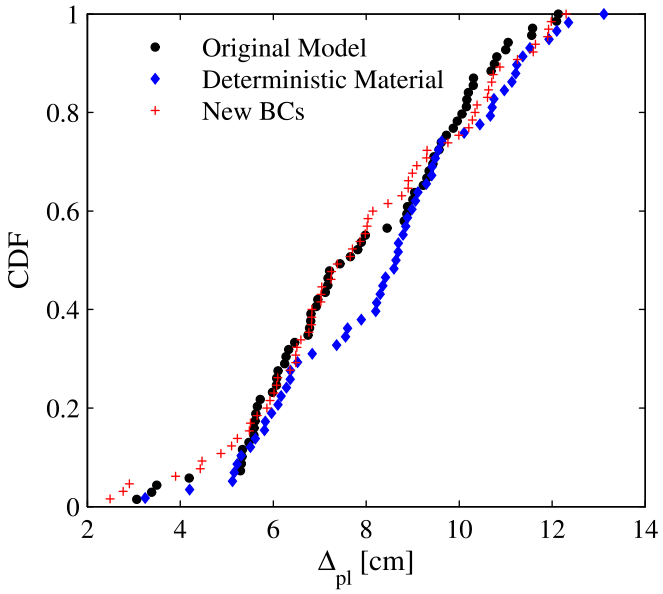

Figure 23. Effects of boundary conditions and material variability on the experimental CDFs of Δ_{pl} for ordinary impacts and KE_m = 1.088 kJ.

In both Figure 22 and Figure 23, the three experimental CDFs are similar, particularly the ones corresponding to the Original Model and the New BCs cases. The CDFs of Δ_{max} and Δ_{pl} corresponding to the Deterministic Material case have a slightly smaller mean than in the other two cases. These results suggest that, in contrast to the number of penetrations and boundary impacts, the variability of the material parameters has a greater influence (albeit overall small) than the boundary conditions on the probability distributions of the *EDP*s relative to ordinary impacts only.

4.4 Damage Analysis Results and Development of Fragility Curves

In the damage analysis phase, the *EDP*s (Δ_{max} and Δ_{pl}) obtained in the structural analysis phase are compared to relevant *DM*s, including a measure of damage to the panel itself, a measure of damage to the window behind the panel, and a measure of complete penetration. Figure 24 graphically represents the failure conditions corresponding to these *DM*s. Figure 24(a) illustrates the limit state corresponding to failure of the panel only. In this scenario, a WBD impact causes the hurricane panel to reach an excessive plastic deformation (i.e., the plastic deformation is enough to render the panel unusable in future storms, yet the maximum deflection of the panel is not enough to damage the window behind it). This failure occurs when the value of the *EDP* Δ_{pl} recorded from the FE model output is larger than or equal to the threshold *DM* ξ_{pl} assumed to warrant replacement of the panel (i.e., $\Delta_{pl} \geq \xi_{pl}$). In this research, it is assumed that ξ_{pl} can be represented as a lognormally distributed random variable with mean $\mu\left(\xi_{pl}\right)$ = 2.500 inches (6.350 cm), and coefficient of variation $\mathrm{COV}\left(\xi_{pl}\right)$ = 0.100. Figure 24(b) illustrates the limit state corresponding to excessive deformation of the panel resulting in the failure of both the panel and the window behind it. In this case, a failure occurs when the *EDP* Δ_{max} obtained from

the FE analysis is larger than or equal to the threshold *DM* ξ_{max}, defined as the minimum distance between the storm panel and the window protected by the panel (i.e., $\Delta_{max} \geq \xi_{max}$). It is assumed that the ξ_{max} can be represented as a lognormally distributed random variable with mean $\mu(\xi_{max})$ = 5.0 inches (12.700 cm), and coefficient of variation $\mathrm{COV}(\xi_{max})$ = 0.150. The statistics of ξ_{pl} and ξ_{max} adopted in this thesis represent realistic values of the means and COVs based on engineering judgment. However, for real-world applications, these statistics should be obtained from statistical data regarding window installation in the hurricane prone region of interest. Figure 24(c) illustrates the complete penetration of the panel and window after WBD impact. A simulation corresponding to a missile penetration is also considered a failure with respect to the other two *DM*s of interest.

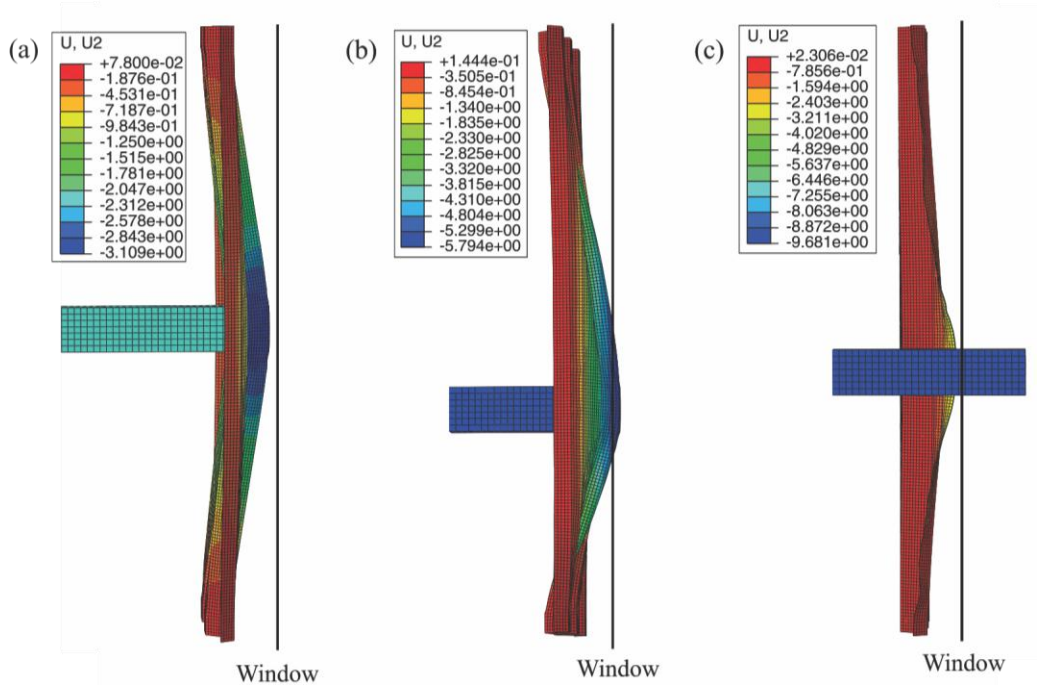

Figure 24. Damage limit states: (a) damage to the storm panel, (b) damage to the window, and (c) penetration of the missile.

Fragility curves are constructed from the data by plotting the probability of failure relative to each *DM* versus its corresponding level of *IM*. These curves represent the CDFs of the relevant *DM*s as functions of KE_m and are presented in Figure 25. Each data point in Figure 25 is representative of 100 stochastic FE simulations at a specific level of the *IM*. Therefore, the probability of failure with respect to each *DM* is the number of total failures out of 100 total trials for each discrete KE_m level. In addition to the fragility curves obtained by modeling both ξ_{pl} and ξ_{max} as random variables (referred to as random threshold (RT) fragility curves), Figure 25 also plots the fragility curves obtained by assuming ξ_{pl} and ξ_{max} equal to their mean values (referred to as deterministic threshold (DT) fragility curves).

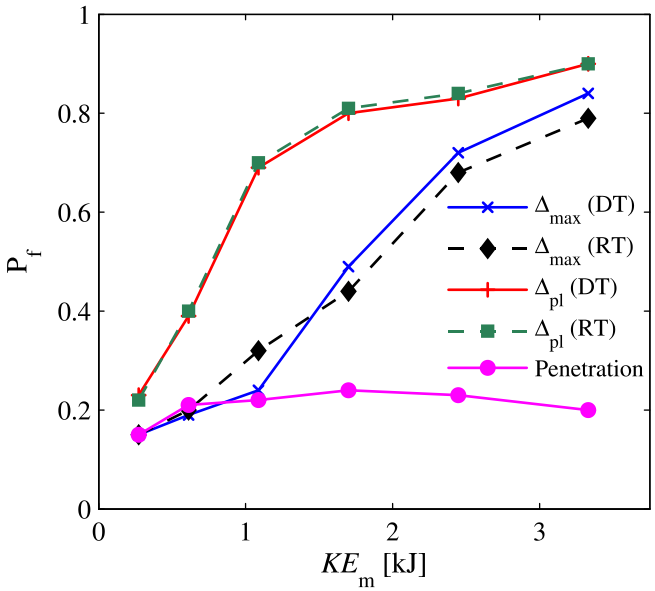

Figure 25: Fragility curves for hurricane protection panels.

In Figure 25, it is observed that (1) the DT and RT fragility curves for the *DM* related to the panel failure (i.e., for the limit state $\Delta_{pl} \geq \xi_{pl}$) are extremely close; (2) the RT fragility curve for the *DM* related to the window failure (i.e., for the limit state $\Delta_{max} \geq \xi_{max}$) is significantly flatter (i.e., it is characterized by a larger dispersion) than the corresponding DT fragility curve; and (3) for low values of KE_m, penetrations are the dominant failure condition. Thus, while the panel

failure is practically insensitive to the randomness of the failure threshold, the window failure condition shows a non-negligible dependence on the variability of the failure threshold.

5 CONCLUSIONS AND RECOMMENDATIONS

This thesis presents the development of windborne debris (WBD) impact fragility curves for building envelope components (BECs) in the context of a performance-based engineering (PBE) methodology for assessment and mitigation of WBD impact hazard produced by hurricanes. These fragility curves provide the probabilistic description of the impact resistance of BECs subject to an impact event described by an appropriate intensity measure (*IM*). Monte Carlo simulation is used in combination with the FE method to propagate the uncertainties from modeling parameters (such as material constitutive parameters and impact location) to engineering demand parameters (*EDP*s), i.e., response parameters computed, in this case, by using dynamic impact analysis of nonlinear FE models of BECs and wooden missiles. Appropriate damage measures (*DM*s) are defined to describe relevant physical states of damage and evaluate the structural performance.

This thesis focuses on BECs with ductile behavior. For this typology of BECs (which includes the aluminum storm panels for window protection used as an application example in this thesis), it is found that the impact kinetic energy, KE_m, is a sufficient *IM*. Three damage states are identified, namely (1) damage to the storm panel (with *EDP* corresponding to the maximum plastic deformation of the panel, Δ_{pl}); (2) damage to the window protected by the storm panel (with *EDP* corresponding to the maximum total deflection of the panel, Δ_{max}); and (3) penetration of the panel by the missile. Three typologies of impacts are identified: (1) boundary impacts, (i.e., impacts whose effects are mainly dependent on the installation details of the storm panel and on the strength of the wall on which the panel is installed); (2) penetrations; and (3) ordinary impacts. For boundary impacts, the values of the *EDP*s are generally very small and, under the assumption that the wall is sufficiently resistant to avoid damage from WBD

impact, correspond to no building damage. For penetrations, the values of the *EDP*s are undetermined and the level of damage to the building is the highest produced by WBD impact. For ordinary impacts, the values of the *EDP*s related to panel damage and window damage show a significant variability and can be described using, e.g., a truncated normal probability distribution. It is observed that impact location has a crucial effect on determining the type of impact and the corresponding damage to the structure. It is shown that a small change in the model's boundary conditions results in a significant reduction of the number of penetrations observed. Therefore, the recommendation is made to include in future building codes a minimum requirement for the overlap between hurricane protection panels and the walls of a structure. This minimum requirement would have the beneficial effect to reduce significantly the probability of penetration of WBDs in buildings with a minimal modification of common practice and a negligible additional cost for the building's owners and the storm panels' producers. It is also shown that, while boundary impacts and penetrations depend mainly on the boundary conditions (i.e., installation details) of the storm panel, the values of the *EDP*s obtained from ordinary impacts show a small but not insignificant dependency on material variability.

Development of fragility curves for BECs plays an integral role in the development of a probabilistic performance-based hurricane engineering (PBHE) framework. The procedure developed in this thesis can be extended to any type of BEC subject to WBD impacts. Further research is needed to identify appropriate *IM*s, *EDP*s, and *DM*s for different typologies of BECs and structural components of structural systems located in hurricane-prone regions.

Based on the research presented in this thesis, the following recommendations for future research are made. (1) In order to confirm the results obtained in this research, an experimental validation must be conducted for aluminum hurricane protection panels with different

installation typologies. The experiments should be conducted using an apparatus capable of launching 2”x4” lumber missiles at the speeds necessary to achieve the levels of KE_m considered in this research (i.e., the air cannon at Louisiana State University). (2) As there are many different types of BECs and WBD impact protection systems with vastly different materials and characteristics, the development of fragility curves for these other types of BECs is crucial. The vulnerabilities of both BECs with brittle materials and ductile materials have been assessed in previous research available in the literature, but there remains a need to assess the vulnerability of BECs with intermediate properties representative of behavior between brittle and ductile. (3) The behavior of BECs impacted by types of WBD other than rod type 2”x4” lumber missiles is not considered in this research. Previous research demonstrates that BECs subjected to WBD impact behave differently depending on the type of the WBD impacting them. Therefore, it is recommended to develop fragility curves for BECs subject to WBD impact by compact and sheet type debris to give a full description of their fragilities in terms of WBD impact. (4) It is also noted that structures are subjected to several different hazards besides WBD impact during a hurricane. There are some sources of hazard which may interact with each other and compound the damage to a structure. A particular area of interest for future research related to WBD impact on BECs is the study of the effects of interaction between WBD impact and wind pressure. (5) The development of overall fully-probabilistic PBHE framework is necessary to rigorously assess the hazards and possible damages to a structure located in a hurricane-prone region. The methodology presented in this thesis for developing fragility curves for BECs subjected to WBD impact can be extended in order to develop a more general overall PBHE framework. Such framework should account for the interaction among different hazards and between hazard and

fragility (e.g., WBD damage to a structure increases the fragility of the structure to wind hazard, and wind damage increases the hazard of WBD impact for surrounding structures).

REFERENCES

[1] National Science Board (NSB). Hurricane warning: the critical need for a national hurricane research initiative. NSB-06-115. National Science Foundation, Arlington, VA; 2007.

[2] Pielke RA, Gratz J, Landsea CW, Collins D, Saunders MA, Musulin R. Normalized hurricane damage in the United States: 1900-2005. Natural Hazards Review 2008;9(1):29-42.

[3] Stewart MJ. Cyclone damage and temporal changes to building vulnerability and economic risks for residential construction. Journal of Wind Engineering and Industrial Aerodynamics 2003;91(5):671-91.

[4] Kentang L. An analysis of the recent severe storm surge disaster events in China. Natural Hazards 2000;21(2):215-23.

[5] Kates RW, Colten CE, Laska S, Leatherman SP. Reconstruction of New Orleans after Hurricane Katrina: a research perspective. Proceedings, National Academy of Sciences 2006;103(40):14653-60.

[6] Holmes J. Windborne debris and damage risk models: a review. Proceedings, Advances in Wind and Structures Conference, Jeju, Korea; May 29-31, 2008.

[7] Li Y, Ellingwood B. Hurricane damage to residential construction in the US: importance of uncertainty modeling in risk assessment. Engineering Structures 2006;28(7):1009-18.

[8] Nowak AS. Report 368. Calibration of LRFD bridge design code. Transportation Research Board, Wasington, D.C.; 1999.

[9] Abu-Farsakh MY, Yu X, Yoon S, Tsai C. Calibration of resistance factors needed in the LRFD design of drilled shafts. Tech. no. FHWA/LA.10/470; 2010.

[10] Kwon O, Kim E, Orton S. Calibration of the live load factor in LRFD bridge design specifications based on state-specific traffic environments. Journal of Bridge Engineering 2010; Accepted, doi:10.1061.

[11] Cornell CA, Krawinkler H. Progress and challenges in seismic performance assessment. PEER Center News 2000;3(2):1-4.

[12] Porter K. An overview of PEER's performance-based earthquake engineering methodology. Proceedings, Conference on Applications of Statistics and Probability in Civil Engineering, San Francisco, California; July 6-9, 2003.

[13] Augusti G, Ciampoli M. First steps towards performance-based wind engineering, Performance of Wind Exposed Structures: results of the PERBACCO project. Firenze University Press, Florence, Italy; 2006.

[14] Petrini F. A probabilistic approach to performance-based wind engineering (PBWE). Ph.D. Dissertation, University of Rome "La Sapienza", Rome, Italy; 2009.

[15] Ciampoli M, Petrini F, Augusti G. A procedure for performance-based wind engineering. Proceedings, International Conference on Structural Safety and Reliability, Osaka, Japan; September 13-17, 2009.

[16] Hamburger RO, Whittaker AS. Considerations in performance-based blast resistant design of steel structures. Proceedings, AISC-SINY Symposium on Resisting Blast and Progressive Collapse. American Institute of Steel Construction, New York; 2003.

[17] Rini D, Lamont S. Performance based structural fire engineering for modern building design. Proceedings, Structures Congress; 2008.

[18] Bertero RD, Vitelmo V. Performance-based seismic engineering: the need for a reliable conceptual comprehensive approach. Earthquake Engineering & Structural Dynamics 2002;31(3):627-52.

[19] Luco N, Cornell CA. Structure-specific scalar intensity measures for near-source and ordinary earthquake ground motions. Earthquake Spectra 2007;23(2):357-92.

[20] Vamvatsikos D, Cornell CA. Developing efficient scalar and vector intensity measures for IDA capacity estimation by incorporating elastic spectral shape information. Earthquake Engineering and Structural Dynamics 2005;34(13):1573-1600.

[21] Baker JW, Cornell CA. A vector-valued ground motion intensity measure consisting of spectral acceleration and epsilon. Earthquake Engineering & Structural Dynamics 2005a;34(10):1193–1217.

[22] Baker JW, Cornell CA. Vector valued intensity measures incorporating spectral shape for prediction of structural response. Journal of Earthquake Engineering 2008;12(4):534-54.

[23] Barbato M, Petrini F, Ciampoli M. A preliminary proposal for a probabilistic performance-based hurricane engineering framework. Proceedings, ASCE Structures Congress, Las Vegas, Nevada; April 14-16, 2011.

[24] Lupoi G, Franchin P, Lupoi A, Pinto P. Seismic fragility analysis of structural systems. Journal of Engineering Mechanics 2006;132(4):385-95.

[25] Gardoni P, Der Kiureghian A, Mosalam KM. Probabilistic models and fragility estimates for bridge components and systems. PEER Center, University of California, Berkeley; 2002.

[26] Brandenberg SJ, Zhang J, Kashighandi P, Huo Y, Zhao M. Demand fragility surfaces for bridges in liquefied and laterally spreading ground. PEER Center, University of California, Berkeley; 2011.

[27] Mackie K, Stojadinovic B. Fragility curves for reinforced concrete highway overpass bridges. Proceedings, 13th World Conference on Earthquake Engineering, Vancouver, Canada; August 1-6, 2004.

[28] Federal Emergency Management Administration (FEMA). Multi-hazard estimation methodology – hurricane model. HAZUS-MH-MR4 Technical Manual. FEMA; 2007, www.fema.gov/plan/prevent/hazus/hz_manuals (August 8, 2011).

[29] Lopez C, Masters FJ, Bolton S, Water penetration resistance of residential window and wall systems subjected to steady and unsteady wind loading. Building and Environment 2011;46(7):1329-42.

[30] Liu JS. Monte Carlo strategies in scientific computing. Springer-Verlag, New York, New York; 2001.

[31] Fernandez G, Masters FJ, Gurley KR. Performance of hurricane shutters under impact by roof tiles. Engineering Structures 2010;32:3384-3393.

[32] Masters FJ, Gurley KR, Shah N, Fernandez G. The vulnerability of residential window glass to lightweight windborne debris. Engineering Structures 2009;32(4):911-21.

[33] Willis JAB, Lee BE, Wyatt TA. A model of windborne debris damage. Journal of Wind Engineering and Industrial Aerodynamics 2002;90(4-5):555-65.

[34] Lin N, Letchford CW, Holmes JD. Investigations of plate-type windborne debris. I. Experiments in full scale and wind tunnel. Journal of Wind Engineering and Industrial Aerodynamics 2006; 94(2):51-76.

[35] Lin N, Holmes JD, Letchford CW. Trajectories of windborne debris and applications to impact testing. Journal of Structural Engineering 2007;133(2):274-82.

[36] NAHB Research Center. Wind-borne debris impact resistance of residential glazing. U.S. Department of Housing and Urban Development, Office of Policy Development and Research, Cooperative Agreement H-21172CA, Washington, D.C; 2002.

[37] Borges A, Lopez RR, Godoy LA, Lopez REZ. Impact of windborne debris on storm shutters. Proceedings, 11th Americas Conference on Wind Engineering. San Juan, Puerto Rico; June 22-26, 2009.

[38] 2012 International Building Code. Country Club Hills, Illinois; 2011.

[39] ASTM Standard E1996. Standard specification for performance of exterior windows, curtain walls, doors and impact protective systems impacted by windborne debris in hurricanes. ASTM International, West Conshohocken, Pennsylvania; 2005.

[40] ASTM Standard E1886. Standard test method for performance of exterior windows, curtain walls, doors, and impact protective systems impacted by missile(s) and exposed to cyclic pressure differentials. ASTM International, West Conshohocken, Pennsylvania; 2005.

[41] Twisdale LA, Vickery PJ, Steckley AC. Analysis of hurricane windborne debris impact risk for residential structures. Report 5303. Applied Research Associates, Raleigh, North Carolina; 1996.

[42] American Society of Civil Engineers (ASCE). Minimum design loads for buildings and other structures. ASCE Standard 7-05. Reston, Virginia; 2006.

[43] Whittaker A, Hamburger R, Mahoney M. Performance-based engineering of buildings for extreme events. Proceedings, AISC-SINY Symposium on Resisting Blast and Progressive Collapse. AISC, New York, New York; December 2003.

[44] Augusti G, Ciampoli M. Performance-based design in risk assessment and reduction. Probabilistic Engineering Mechanics 2008; 23(4):496-508.

[45] Federal Emergency Management Administration (FEMA). NEHRP guidelines for the seismic rehabilitation of buildings. Report no. FEMA 273. Prepared by the Applied Technology Council for FEMA, Washington, D.C.; 1997.

[46] Applied Technology Council (ATC). Development of next-generation performance-based seismic design procedures for new and existing buildings, ATC-58. Applied Technology Council, Redwood City, CA; 2005.

[47] Comartin CD. Applications of performance-based engineering to risk management decisions. Proceedings, International Workshop on Performance-Based Seismic Design Concepts and Implementation. Bled, Slovenia, June 28 – July 1, 2004.

[48] Hamburger RO. Development of next-generation performance-based seismic design guidelines. Proceedings, International Workshop on Performance-Based Seismic Design Concepts and Implementation. Bled, Slovenia, June 28 – July 1, 2004.

[49] Pinho R. Performance and displacement-based earthquake loss estimation of urban areas. Proceedings, International Workshop on Performance-Based Seismic Design Concepts and Implementation. Bled, Slovenia, June 28 – July 1, 2004.

[50] Aktan AE, Ellingwood BR, Kehoe B. Performance-based engineering of constructed systems. The ASCE SEI Technical Committee, Performance of Structures Technical Activities Division, Reston, VA; 2006.

[51] Porter KA, Beck JL, Shaikhutdinov RV. Investigation of sensitivity of building loss estimates to major uncertain variables for the Van Nuys testbed, PEER Report 2002/03. Pacific Earthquake Engineering Research Center, Richmond, CA; 2002.

[52] Porter KA, Beck JL, Seligson HA, Scawthorn CR, Tobin LT, Young R, Boyd T. Improving loss estimation for woodframe buildings. Draft final report, volume 2. Consortium of Universities for Research in Earthquake Engineering, Richmond, CA; 2001.

[53] Beck JL, Porter KA, Shaikhutdinov R, Moroi T, Tsukada Y, Masuda M. Impact of seismic risk on lifetime property values. Final report, CUREE-Kajima joint research program phase IV. Consortium of Universities for Earthquake Engineering Research, Richmond, CA; 2002.

[54] Shome NC, Cornell CA, Bazzurro P, Caraballo EJ. Earthquakes, records, and nonlinear responses. Earthquake Spectra 1998;14(3):469-500.

[55] Ang AH-S, Tang WH. Probability concepts in engineering planning and design. Volume 1, John Wiley & Sons, Inc., New York; 1975.

[56] ABAQUS standard and explicit user's manuals. Version 6.8. Dassault Systemes Simulia Corp., Providence, Rhode Island, USA; 2008.

[57] AGI Group. Storm panels - architectural and engineering drawings. 2006. Last modified March 2011. http://www.stormshutters.com/storm-panels/drawings.html. Accessed March 10, 2011.

[58] Roeder BA, Sun CT. Dynamic penetration of alumina/aluminum laminates: experiments and modeling. International Journal of Impact Engineering 2001;25(2):169-85.

[59] Laursen TA. Computational contact and impact mechanics: fundamentals of modeling interfacial phenomena in nonlinear finite element analysis. Springer-Verlag, Berlin; 2002.

[60] Belytschko T, Liu WK, Moran B. Nonlinear finite elements for continua and structures. John Wiley & Sons Ltd., West Sussex, England; 2000.

[61] Kaufman JG. Properties of aluminum alloys. ASM International, Materials Park, Ohio; 2008.

[62] Forest Products Laboratory. Wood handbook – wood as an engineering material. Department of Agriculture, Forest Service, Forest Products Laboratory, General Technical Report FPL-GTR-190, Madison, Wisconsin; 2010.

[63] Kececioglu D. Reliability and life testing handbook. Volume 1, Prentice Hall, Englewood Cliffs, New Jersey; 1993.

APPENDIX A SAMPLE RESULTS OF MCS

This appendix presents the 100 sampled values of each random variable considered in this research corresponding to the original model case for KE_m = 0.612 kJ. These values are obtained using Monte Carlo simulation. In each figure, the theoretical mean value and 10% and 90% fractiles are also shown for each random variable.

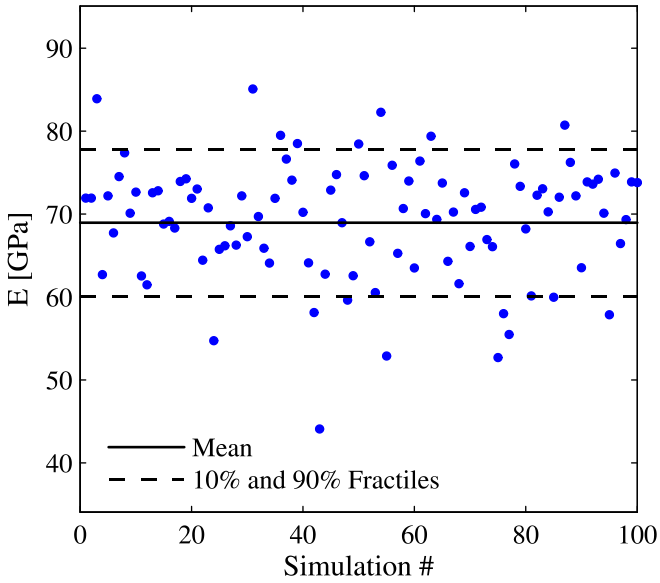

Figure 26. MCS results for aluminum Young's modulus.

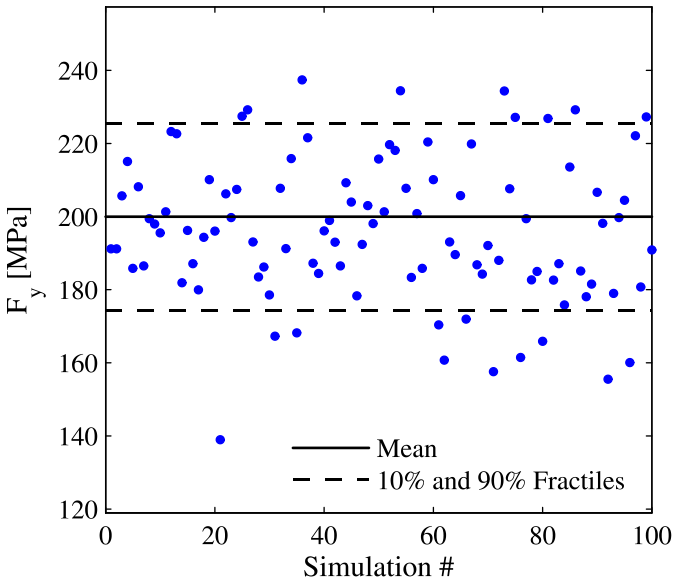

Figure 27. MCS results for aluminum yield stress.

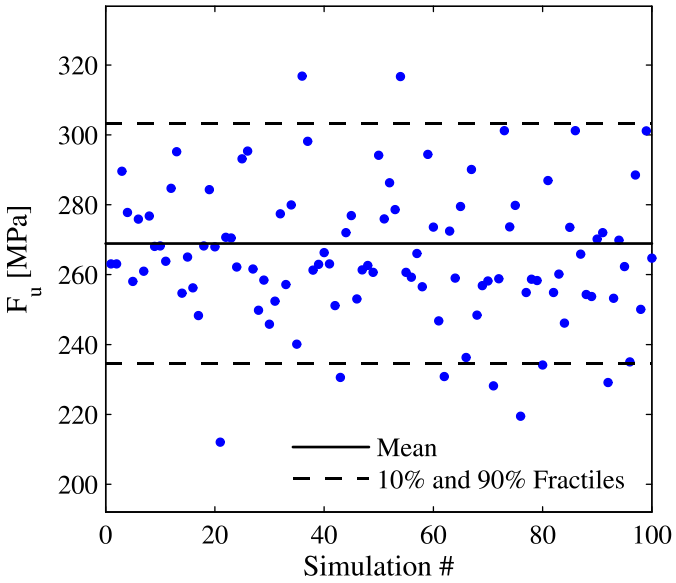

Figure 28. MCS results for aluminum ultimate stress.

APPENDIX B EXPERIMENTAL AND FITTED CDFS

This appendix provides the comparison between the reduced CDFs (i.e., corresponding to ordinary impact only) experimentally obtained from FE simulations and the normal, lognormal, and truncated normal theoretical distributions with parameters estimated from the sample data. These CDFs are used to perform a modified Kolmogorov-Smirnov goodness of fit test to determine which theoretical distribution best describes each of the experimentally obtained data sets (i.e., corresponding to Δ_{max} and Δ_{pl} for ordinary impacts at each level of KE_m considered in this research).

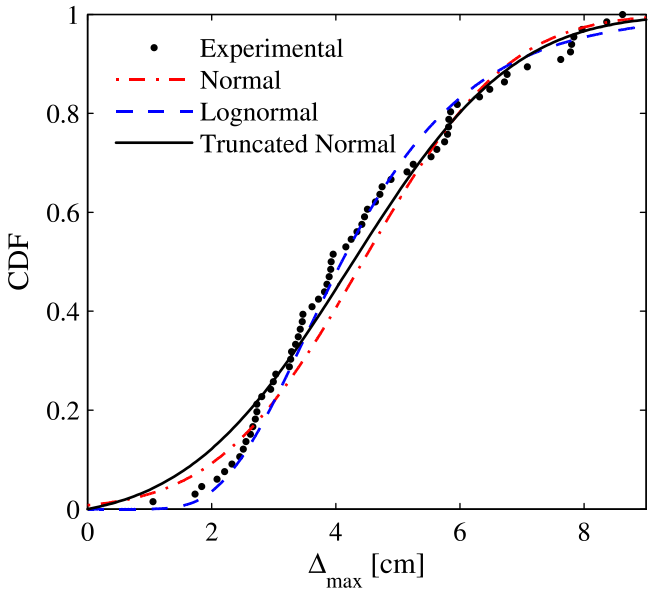

Figure 29. Experimental and fitted CDFs of Δ_{max} for ordinary impacts and KE_m = 0.272 kJ.

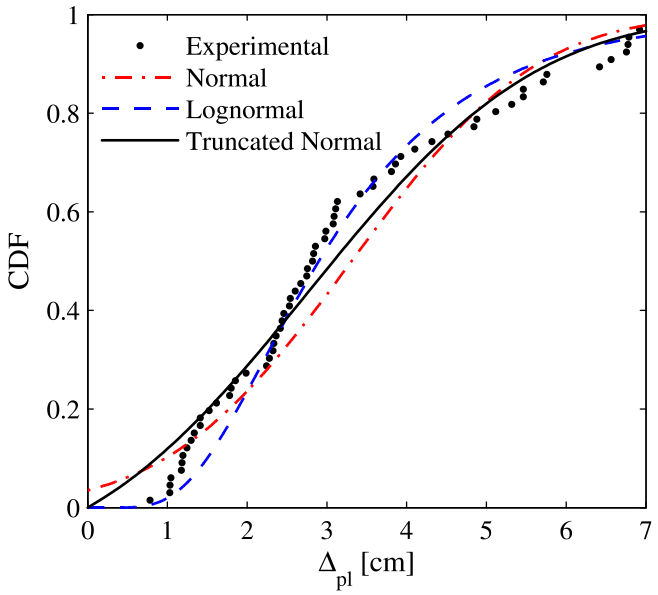

Figure 30. Experimental and fitted CDFs of Δ_{pl} for ordinary impacts and KE_m = 0.272 kJ.

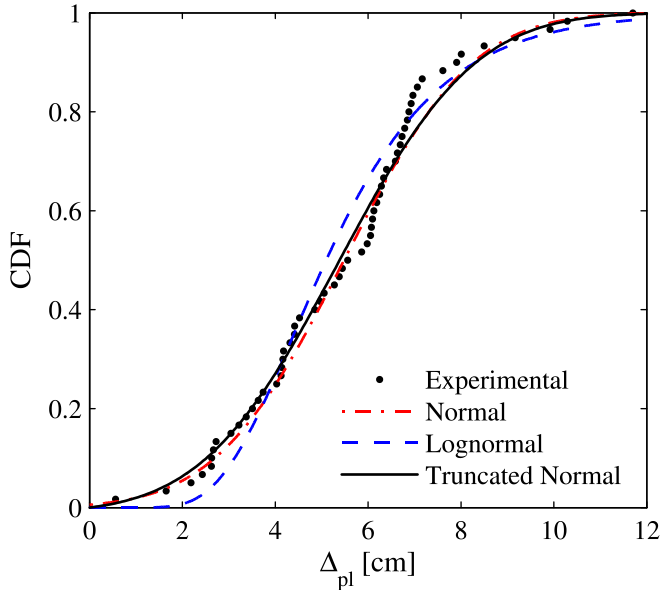

Figure 31. Experimental and fitted CDFs of Δ_{pl} for ordinary impacts and KE_m = 0.612 kJ.

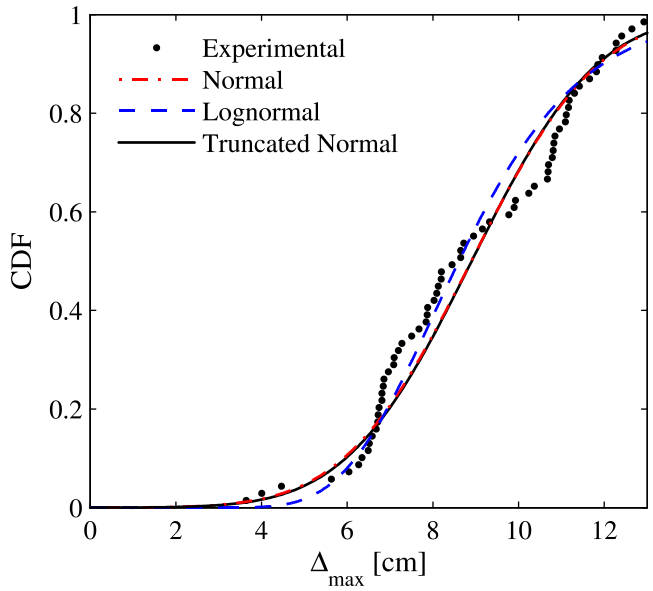

Figure 32. Experimental and fitted CDFs of Δ_{max} for ordinary impacts and KE_m =1.088 kJ.

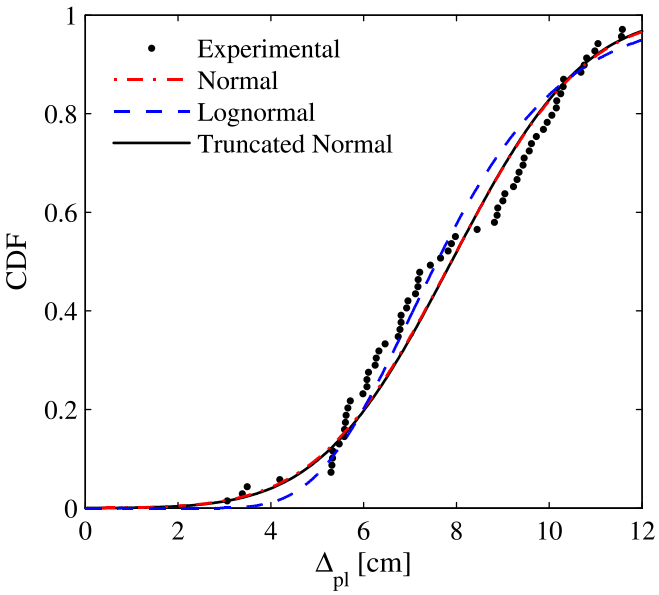

Figure 33. Experimental and fitted CDFs of Δ_{pl} for ordinary impacts and KE_m = 1.088 kJ.

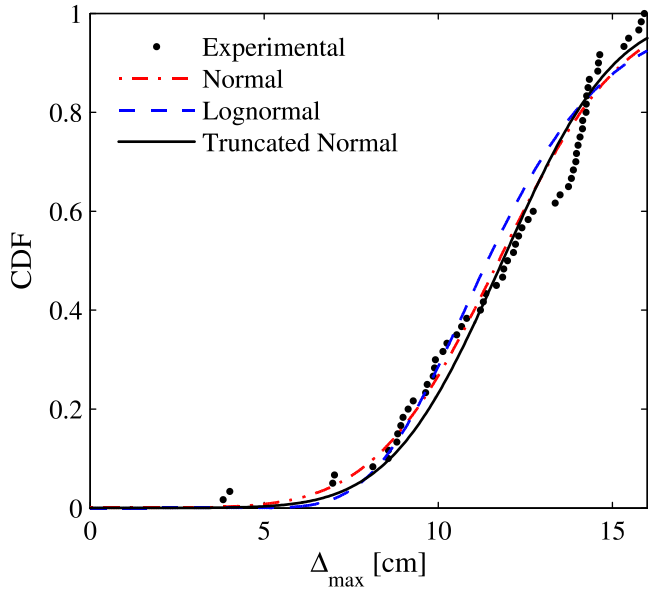

Figure 34. Experimental and fitted CDFs of Δ_{max} for ordinary impacts and KE_m = 1.700 kJ.

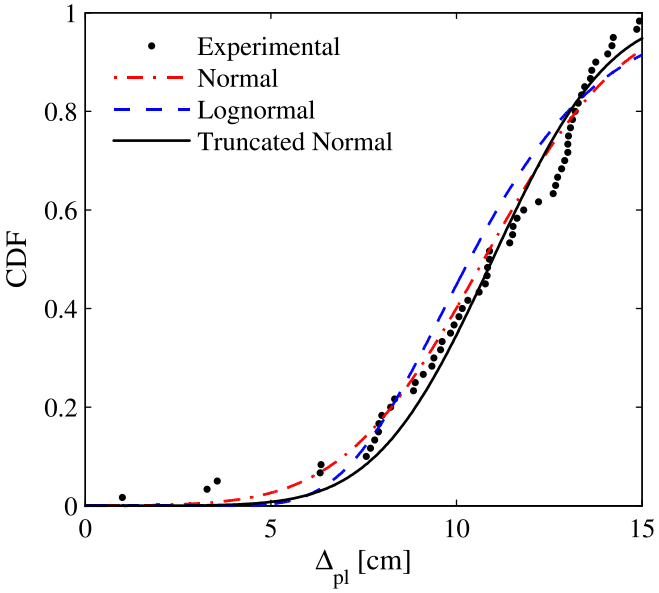

Figure 35. Experimental and fitted CDFs of Δ_{pl} for ordinary impacts and KE_m = 1.700 kJ.

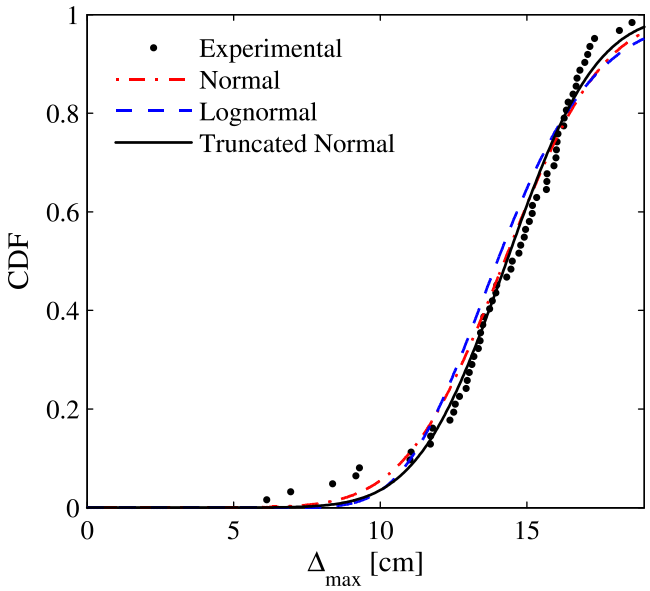

Figure 36. Experimental and fitted CDFs of Δ_{max} for ordinary impacts and KE_m = 2.448 kJ.

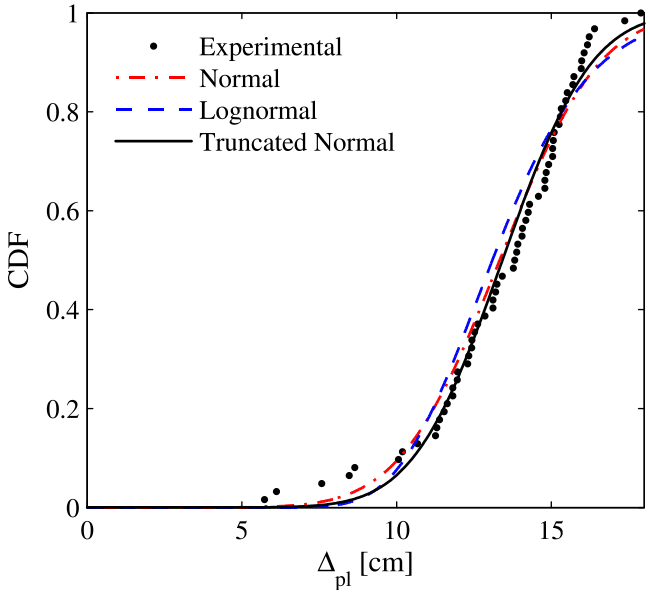

Figure 37. Experimental and fitted CDFs of Δ_{pl} for ordinary impacts and KE_m = 2.448 kJ.

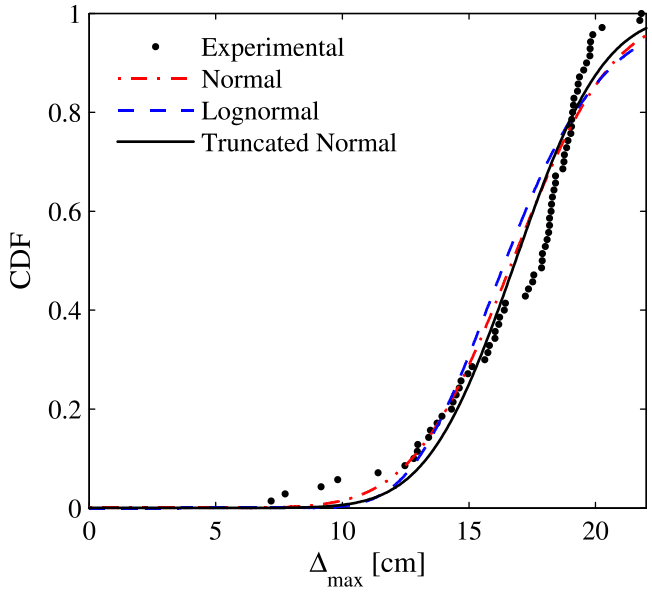

Figure 38. Experimental and fitted CDFs of Δ_{max} for ordinary impacts and KE_m = 3.331 kJ.

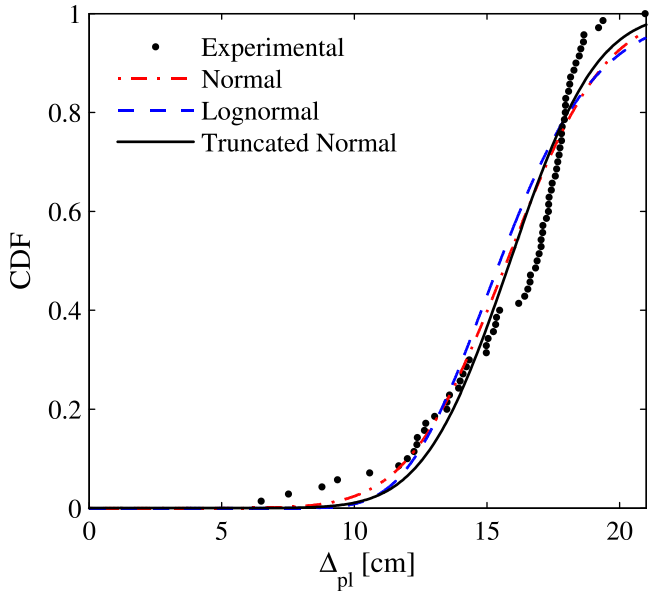

Figure 39. Experimental and fitted CDFs of Δ_{pl} for ordinary impacts and KE_m = 3.331 kJ.

VITA

Alexander Henry Herbin was born on June 18th, 1986 in New Rochelle, New York. He graduated from Slidell High School in Slidell, Louisiana in May, 2004 and began his undergraduate studies at Louisiana State University in the fall of the same year. He received his Bachelor of Science degree in Civil Engineering from Louisiana State University in December of 2008. After graduating, he began his graduate studies at Louisiana State University in January 2009. He is expected to receive his Master of Science degree in Civil Engineering in December of 2011.